

NASA REPORT NO. CR 174926

# ARVIN/CALSPAN

*A HYBRID NUMERICAL TECHNIQUE FOR  
PREDICTING THE AERODYNAMIC AND  
ACOUSTIC FIELDS OF ADVANCED TURBOPROPS*

Contract No. NAS3-23699

April 1985

FINAL REPORT

CALSPAN REPORT NO. 7157-A-1

Prepared by:

G.F. Homicz and J.R. Moselle  
PHYSICAL SCIENCES DEPARTMENT

Prepared for:

NATIONAL AERONAUTICS AND SPACE ADMINISTRATION  
LEWIS RESEARCH CENTER  
CLEVELAND, OHIO 44135

## FOREWORD

This is the final report documenting the results of a theoretical program to predict the aerodynamic and acoustic performance of advanced turboprops, sponsored by the NASA Lewis Research Center. The program extended from April 1983 to March 1985, with Dr. Kenneth Baumeister serving as Technical Monitor.

Dr. Paul V. Marrone, Head of the Physical Sciences Department, has overall responsibility for management and review of all technical programs within the department. It was originally envisioned that Dr. William J. Rae would serve as Principal Investigator, with assistance from Drs. Gregory F. Homicz, Joseph P. Nenni, and John A. Lordi. Shortly after the program began, the departure of Drs. Rae, Nenni and Lordi led to Dr. Homicz being appointed Principal Investigator. To aid him in the technical effort, Calspan obtained the services of Prof. A. Seybert of the University of Kentucky as a subcontractor. Prof. Seybert had responsibility for the outer linearized acoustic analysis and the preparation of Section 4 and portions of Section 5 of this report. We wish to thank Dr. L. Bober, M. Celestina, and H. Huynh of NASA Lewis for their generous help in familiarizing us with the NASPROP-E code and their system.

## ABSTRACT

A hybrid numerical procedure is presented for the prediction of the aerodynamic and acoustic performance of advanced turboprops. Because the relative tip speed at design is typically supersonic, one must anticipate the presence of shock waves as well as transonic three-dimensional effects in the immediate vicinity of the blades. The strong rotational character of such flows warrants the use of the inviscid nonlinear Euler equations in predicting aerodynamic performance. In the outer flow regime away from the propeller such effects have decayed significantly; here the primary concern is the sound being propagated to the farfield. Hence in this region a linearized acoustic analysis is justified.

The present investigation proposes a hybrid scheme which in principle leads to a consistent simultaneous prediction of both fields. In the inner flow a finite difference method, the Approximate-Factorization Alternating-Direction-Implicit (ADI) scheme, is used to solve the nonlinear Euler equations. In the outer flow the linearized acoustic equations are solved via a Boundary-Integral Equation (BIE) method. The two solutions are iteratively matched across a fictitious interface in the flow so as to maintain continuity. At convergence the resulting aerodynamic load predictions will automatically satisfy the appropriate "free-field" boundary conditions at the edge of the finite difference grid, while the acoustic predictions will reflect the "back-reaction" of the radiated field on the magnitude of the loading source terms, as well as refractive effects in the inner flow.

The equations and logic needed to match the two solutions are developed and the computer program implementing the procedure is described. Unfortunately, no converged solutions were obtained, due to the unexpectedly large running times. The reasons for this are discussed and several means to alleviate the situation are suggested.

## TABLE OF CONTENTS

<u>Section</u>	<u>Title</u>	<u>Page</u>
	FOREWORD .....	ii
	ABSTRACT .....	iii
	LIST OF ILLUSTRATIONS .....	v
1	INTRODUCTION .....	1
2	INNER NONLINEAR AERODYNAMIC MODEL .....	4
	Grid Transformation .....	4
	Transformed Equations .....	5
	Numerical Algorithm .....	8
	Initial and Boundary Conditions .....	9
3	MATCHING ACROSS THE INTERFACE .....	12
	Evaluation of Normal Pressure Gradient at Interface .....	12
	Transformation from Mean Flow to Static Flow .....	16
	Update to Boundary Conditions .....	20
4	OUTER LINEARIZED ACOUSTIC MODEL .....	22
	Review of the BIE Method .....	22
	Axisymmetric Formulation .....	26
	Numerical Implementation .....	28
	Calculation of Farfield Sound Pressure .....	30
	The Interior Eigenfrequency Problem .....	30
	Attempts to Circumvent the Eigenfrequency Problem .....	32
5	PROGRAM CALPROP .....	34
	Changes to NASPROP-E Routines .....	34
	New Routines Unique to CALPROP .....	39
	Modified Mesh for the BIE .....	43
	Description of Routines in BIE .....	44
	Description of Important Parameters in BIE .....	48
6	RESULTS .....	51
7	CONCLUSIONS AND RECOMMENDATIONS .....	57
	REFERENCES .....	61
	NOMENCLATURE .....	63

LIST OF ILLUSTRATIONS

<u>Figure</u>	<u>Title</u>	<u>Page</u>
1	Finite Difference Grid in $z, r$ Plane	6
2	Interface Surface $S$ Across Which Inner and Outer Flow Solutions are Matched	13
3	Radiation from a Surface $S_0$ into an Exterior Region $V$	23
4	A Simply-Connected Axisymmetric Body	27
5	Overall Structure of CALPROP	35
6	Original and Modified Node Placements	45
7	Hierarchy Chart for the BIE Package	47
8	Input Data for Demonstration Case	52

Section 1  
INTRODUCTION

The past two or three decades have witnessed a progression in the commercial aviation fleet from propeller to turbojet, and most recently, to turbofan-powered aircraft. The transition has been motivated primarily by the desire for increased speed, reduced cabin vibration, and relatively simpler design. Early turbojet engines were rather noisy, due to the very high exit velocities of the turbulent exhaust jet. This eventually led to the turbofan engine, whose exhaust velocity (and resultant noise) is much lower. To compensate for the reduced jet thrust, a significant fraction of the inlet air is made to bypass the core engine and flows instead through a ducted fan, which generates a significant portion of the thrust.

In recent years the need for increased fuel efficiency has prompted reconsideration of the propeller as a viable alternative. Operation at a typical cruise condition ( $M = 0.8$  at 30,000 ft.) usually means blade relative tip speeds which are in the transonic/low supersonic regime. The performance degradation and "buzz-saw" noise produced by conventional turboprops at these conditions preclude their use. Recent advances in our understanding of such flows, and improvements in manufacturing techniques, have driven propeller design in the direction of using many smaller diameter, thinner blades, with a highly swept planform. The similarity to an unducted fan is obvious, hence the name "propfan".

While wind-tunnel as well as flight tests on scale models have confirmed the propulsive efficiency of modern propfan design, the noise they create is still a major concern. Most noise prediction methodologies model the blades as distributions of source and dipole acoustic singularities. The magnitude of these singularities is determined by the blades' thickness and loading distributions, respectively. In principle the geometric thickness distribution is a given, but the loads themselves require another whole prediction methodology, which for advanced propfans is generally a numerical algorithm of some sort. Usually the numerical solution is extended only a finite distance from the propeller, where uniform free-stream conditions are assumed to exist. This assumption is clearly inconsistent with acoustic

radiation to the farfield. Such an approach thus completely neglects any coupling between the aerodynamic and acoustic field, i.e. the "back-reaction" of the radiative field on the source mechanism.

Comparisons of such noise predictions against available wind-tunnel and flight test acoustic data, e.g. Refs. 1 and 2, show uneven agreement. The Sound Pressure Level (SPL) for both theory and experiment exhibits a nearly linear increase with increasing tip speed in the subsonic regime. However, as the relative tip Mach number passes through unity, the data tend to level off at a plateau, while the predicted SPL continues to rise. It is the discrepancy between theory and experiment in the transonic regime which this program is intended to address. Specifically, we hope to determine whether a direct coupling of the aerodynamic and acoustic fields in the theory would improve the agreement.

For propeller flows which are subsonic at the hub and supersonic at the tip, strong transonic and nonlinear effects must be anticipated, including three-dimensionality, swirl, and even shock waves. These phenomena dictate the solution of the three-dimensional, nonlinear, inviscid Euler equations if accurate aerodynamic predictions are required. For this purpose we have chosen as our starting point the NASPROP-E computer code written by Chaussee and Kutler (Ref. 3). This choice was dictated by the code's ready availability on the NASA Lewis CRAY system, lack of proprietary restraints on its use or modification, and its demonstrated success in treating advanced propfan configurations (Ref. 4).

NASPROP-E solves the Euler equations using a finite-difference algorithm on a boundary-conforming grid. In principle the grid and solution could be extended to the acoustic farfield, but in practice this would soon stretch storage requirements and CPU times to the breaking point. Out of necessity the outer boundary of the grid is placed a finite distance, say several blade diameters, away from the propeller where the boundary conditions are only approximated by undisturbed free-stream values.

On the other hand, one expects intuitively that the nonlinear effects necessitating the use of the full Euler equations are likely to be dominant

only in the immediate vicinity of the blades. In the farfield, where the propagation of acoustic waves is the prime concern, an analysis based on the linearized flow equations should suffice. The latter lend themselves to semi-analytical methods which have a less voracious appetite for computer resources. This suggests a hybrid methodology in which NASPROP-E is used in the inner flow and matched across some suitably chosen interface to a linearized model of the outer flow.

The scheme chosen here for the outer flow is the Boundary-Integral Equation (BIE) method (Ref. 5). As the name suggests, it is based on converting the partial differential equations to an equivalent integral equation on the interface. The number of spatial dimensions is thus reduced from three to two. As envisioned here, the NASPROP-E solution in the inner flow is used to compute the pressure gradient  $\partial p / \partial n$  ( $n$  being normal to the interface). This is used as the inner boundary condition for the outer flow solution. The latter will uniquely determine a new  $p$  distribution on the interface, fully consistent with the appropriate radiation condition at infinity. This new  $p$  distribution is then used as the outer boundary condition on a new calculation of the inner flow. This procedure is repeated until convergence is reached, as evidenced by continuity of pressure and its normal derivative across the interface. After convergence, the SPL at any point in the outer flow is available as a simple quadrature of  $p$  and  $\partial p / \partial n$  (which are now known) over the interface.

The discussion in the following sections proceeds logically from the propeller outwards. Section 2 gives an overview of the equations, variables, and algorithm used in NASPROP-E. Section 3 discusses how this solution is matched across the interface to the BIE solution, which in turn is discussed in Section 4. The overall structure of the combined code, termed CALPROP, is presented in Section 5 along with a description of the additional inputs and outputs. Large computer run times have thwarted efforts to get a converged solution, the reasons for which are discussed in Section 6. Section 7 closes with the major conclusions from this study and suggestions for future research.

Section 2  
INNER NONLINEAR AERODYNAMIC MODEL

As noted in the Introduction, advanced propfan configurations can be expected to exhibit strong rotational flow effects, as well as shock waves. For this reason a solution of the full nonlinear, inviscid, three-dimensional Euler equations is needed in the immediate vicinity of the blades. As our starting point, we chose the NASPROP-E code developed by Chaussee and Kutler (Ref. 3). This source code was readily available and working on the NASA Lewis CRAY system, and has been successfully used to analyze configurations of interest here (Ref. 4).

Actually, the overall package is a collection of three stand-alone programs, each designed to do a different task in the analysis sequence. The first is a mesh generation program which takes the propfan/nacelle geometry as input and produces a suitable boundary-conforming grid. This grid is used as input to the flowfield analysis program, which solves the equations and stores the full three-dimensional solution at all grid points onto a disk file. The last step is the data reduction program which reads the solution on file and computes force and moment coefficients, generates plots of selected quantities, etc. The flowfield analysis program is by far the most complex and time consuming. It is this portion that we are primarily concerned with here, with the exception of one small change noted below in connection with the mesh generation code.

As NASPROP-E has been documented elsewhere, we give here only an overview sufficient to introduce certain variables and concepts. We also discuss what modifications were found necessary to allow interaction with the outer solution field.

Grid Transformation

It is assumed that the inlet flow, at subsonic Mach number,  $M$ , is uniform. Hence to an observer in a blade-fixed reference frame  $(z, r, \phi)$  the flow appears steady, and it is in such a frame that the equations are solved.

Further, since all of the B blades are assumed identical, it is only necessary to solve for the flow through one blade passage, say  $0 \leq \phi \leq 2\pi/B$ . To facilitate implementation of the blade and nacelle boundary conditions, the flow is mapped into computational coordinates,

$$\begin{aligned}\xi &= \xi(z, r, \phi, t) \\ \eta &= \eta(z, r, \phi, t) \\ \zeta &= \zeta(z, r, \phi, t) \\ \tau &= t\end{aligned}\tag{2-1}$$

The transformation is boundary-conforming, i.e., the flow boundaries in the computational domain all lie along constant values of one of the coordinates. In this domain the flow occupies a rectangular prism, within which a uniform Cartesian grid is employed. Such a transformation makes it easy to adapt any number of finite-difference algorithms to the solution. It also allows one to "bunch up" grid points in regions of strong gradients without compromising the accuracy of the difference scheme.

A cross-section in the  $(z, r)$  plane of the difference grid used here is shown in Fig. 1. This displays the non-uniform curvilinear grid in physical space corresponding to a uniform Cartesian grid in  $\xi$  and  $\eta$ . The corresponding integer indices are J and K, respectively. J = 1 represents the horizontal stagnation streamline coming in from the left. Higher values of J are the lines rotating to the right, with J = JA denoting the specific  $\xi =$  constant line intersecting the upper left corner of the grid. The vertical outflow boundary is denoted by J = JMAX. Note the bunching near the stagnation point and the blade leading and trailing edges. The intersecting grid lines are for  $\eta$  and K constant; K = 1 is the nacelle surface, while K = KMAX along the vertical inflow boundary and the horizontal cylindrical sidewall. In the azimuthal direction, L is the index for coordinate  $\zeta$  (not shown in Fig. 1, see Ref. 4); L = 1 lies along the blades' suction surface, and L = LMAX along the blades' pressure surface.

### Transformed Equations

In the computational space the Euler equations can still be written in weak-conservation law form as follows:

$$Q_\tau + E_\xi + F_\eta + G_\zeta + H = 0\tag{2-2}$$

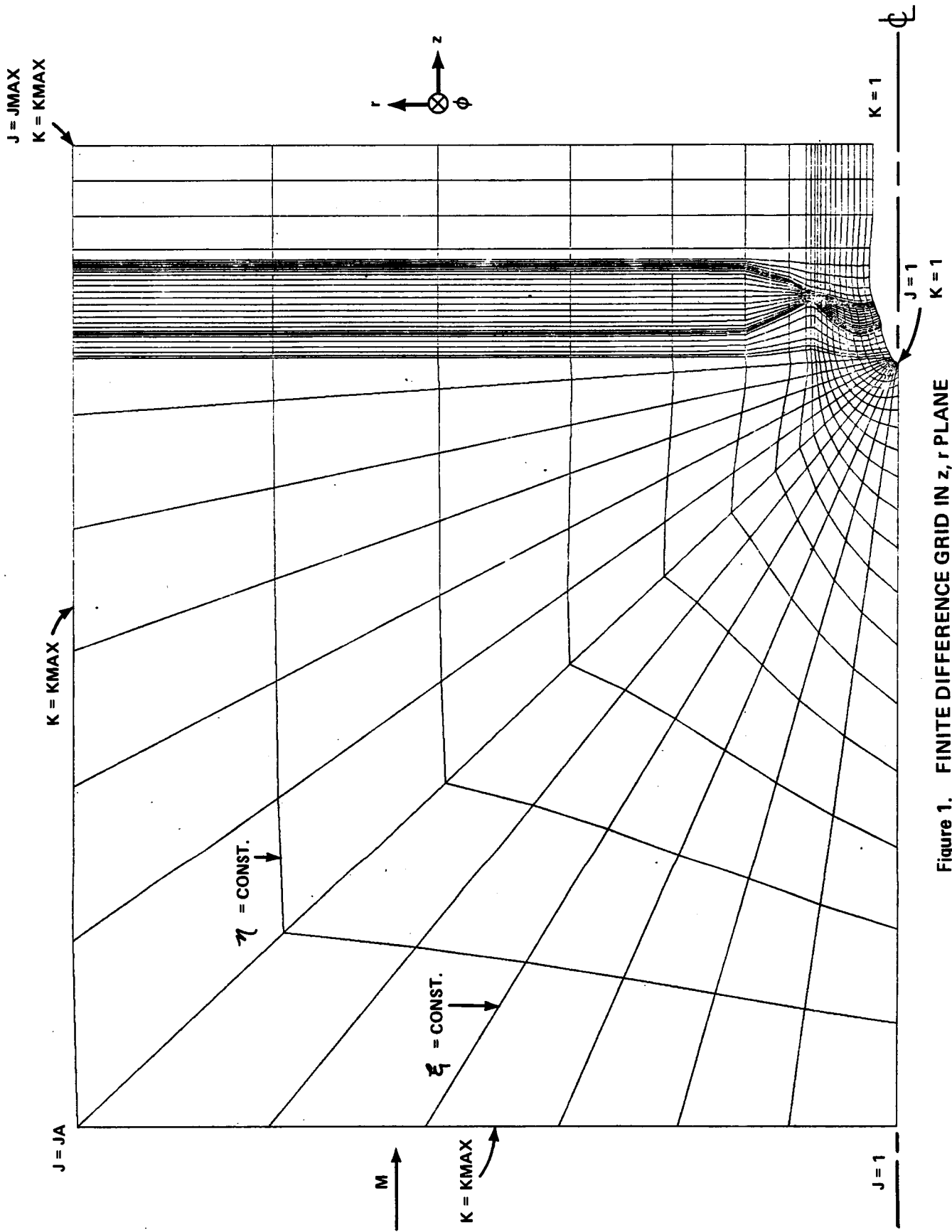


Figure 1. FINITE DIFFERENCE GRID IN  $z, r$  PLANE

where subscripts are used to denote differentiation. Q is a column vector consisting of the unknowns,

$$Q = J^{-1} [\rho, \rho u, \rho v, \rho w, e]^T \quad (2-3)$$

where  $\rho$  is the fluid density, (u, v, w) the velocity components in the (z, r,  $\phi$ ) directions, respectively, and e is the total energy per unit volume defined by

$$e = \frac{p}{(\gamma-1)} + \frac{\rho(u^2 + v^2 + w^2)}{2} \quad (2-4)$$

where p is the pressure. The quantity J is the Jacobian of the transformation defined in Eq. (2-1), i.e.

$$J = \frac{\partial(\xi, \eta, \zeta)}{\partial(z, r, \phi)} \quad (2-5)$$

and  $\gamma$  is the ratio of specific heats for an ideal gas.

Before going further, it should be noted that all variables in the code have been nondimensionalized. Lengths are normalized by the propeller diameter, D. Pressure and density are normalized by their freestream values,  $p_\infty$  and  $\rho_\infty$ . Velocities are normalized by  $a_\infty/\sqrt{\gamma}$ , where  $a_\infty$  is the free-stream sound speed,  $\sqrt{\gamma p_\infty/\rho_\infty}$ . Time is normalized by  $D\sqrt{\gamma}/a_\infty$ . Finally, from Eq. (2-4) the energy per unit volume is also normalized by  $p_\infty$ .

The quantities E, F and G are the column flux vectors in the  $\xi$ ,  $\eta$  and  $\zeta$  directions defined in terms of the unknowns as,

$$\begin{aligned} E &= J^{-1} [\rho U, \rho u U + p \xi_z, \rho v U + p \xi_r, \rho w U + p \xi_\phi/r, (e+p)U - p \xi_t]^T \\ F &= J^{-1} [\rho V, \rho u V + p \eta_z, \rho v V + p \eta_r, \rho w V + p \eta_\phi/r, (e+p)V - p \eta_t]^T \\ G &= J^{-1} [\rho W, \rho u W + p \zeta_z, \rho v W + p \zeta_r, \rho w W + p \zeta_\phi/r, (e+p)W - p \zeta_t]^T \end{aligned} \quad (2-6)$$

Here (U, V, W) are the contravariant velocity components in the ( $\xi$ ,  $\eta$ ,  $\zeta$ ) directions, respectively:

$$\begin{aligned}
U &= \xi_t + u\xi_z + v\xi_r + w\xi_\phi/r \\
V &= \eta_t + u\eta_z + v\eta_r + w\eta_\phi/r \\
W &= \zeta_t + u\zeta_z + v\zeta_r + w\zeta_\phi/r
\end{aligned}
\tag{2-7}$$

The undifferentiated source term H is given by

$$H = (Jr)^{-1} [\rho v, \rho uv, \rho(v^2 - w^2), 2\rho vw, (e + p)v]^T
\tag{2-8}$$

The metrics of the transformation appearing in Eqs. (2-6) and (2-7) can also be evaluated in the computational space using the chain rule, e.g.

$$\begin{aligned}
\xi_z &= J(r_\eta \phi_\zeta - \phi_\eta r_\zeta) \\
\xi_r &= J(\phi_\eta z_\zeta - z_\eta \phi_\zeta) \\
\xi_\phi &= J(z_\eta r_\zeta - r_\eta z_\zeta)
\end{aligned}
\tag{2-9}$$

and similarly for the  $\eta$  and  $\zeta$  metrics.

### Numerical Algorithm

The vector Eq. (2-2) is a shorthand for 5 scalar equations representing, respectively, conservation of mass, conservation of momentum (3 components), and conservation of energy. Note that the time derivative has been retained even though we seek the steady-state solution. This renders the equations hyperbolic and thus amenable to a time-marching algorithm. That is, the solution is integrated from some (arbitrary) initial condition through a sequence of finite time steps until all transients have decayed. This asymptotic field is then the desired steady-state solution.

The use of an explicit finite-difference algorithm, though straightforward, is hampered by the very small time steps required to maintain numerical stability when small grid spacings are present. This is particularly nettlesome in applications such as the present, where the transients are not of interest, and we wish to converge to the steady solution as quickly as possible. For this reason NASPROP-E employs an implicit marching algorithm. Though more operations are required at each time step, implicit schemes allow greatly increased step sizes without sacrificing stability. The net result is a significant savings in CPU time.

The particular scheme used in NASPROP-E is the Approximate-Factorization Alternating-Direction-Implicit (ADI) scheme in so-called "delta" form (Refs. 6, 7). Basically, after applying differencing formulae to Eq. (2-2), the resulting three-dimensional spatial difference operator is factored into the product of three one-dimensional operators. Each of these operators represents a block-tridiagonal matrix. The latter can be inverted one at a time sequentially, a significant savings in both storage and time requirements compared with inverting the much larger matrix for the full three-dimensional operator. A method for speeding the calculation even more through further diagonalization of the block matrix structure (Refs. 8, 9) is also used. For more details on the Approximate-Factorization ADI algorithm and its implementation in NASPROP-E, see Refs. 3, 4, 6-9. No changes to this part of the code were made during the present investigation.

#### Initial and Boundary Conditions

The usual initial condition when starting a case from scratch is to set all the flow variables in the vector  $Q$  equal to their free-stream values. Optionally, one can also start the calculation using the flowfield solution stored as the result of a previous run. No changes have been made to the code in this regard (Section 4.4 of Ref. 3).

The boundary conditions used are those appropriate to an inviscid calculation. Since the blades and nacelle are impermeable the surface tangency condition is invoked, i.e., the velocity normal to the surface must be zero. In the computational space the blades map to a surface of constant  $\zeta$ , so that the corresponding contravariant velocity,  $W$ , must vanish. Similarly, the nacelle maps to a surface of constant  $\eta$ , along which the contravariant velocity  $V$  must be zero. Details of how these are enforced may be found in Ref. 3; no changes were made for the present application.

As originally written, the outer boundary of the NASPROP-E grid was not as depicted here in Fig. 1. The upstream portion, rather than terminating in a flat vertical surface, consisted of a hemispherical cap of the same radius as the downstream cylindrical portion. This will be referred to as the hemisphere-cylindrical grid. On the hemispherical cap and cylindrical sidewall,

K = KMAX, free-stream values for all the flow quantities were imposed for all time. On the vertical downstream outflow boundary (J = JMAX) only the pressure was assumed to have returned to a constant value of  $p_\infty$ . Significant variations in the velocity field must be expected, however, because of the added momentum and swirl imparted to the flow. Appropriate values for the velocity components were computed using the Method of Characteristics (MOC); see Ref. 3 for details. The density was obtained from the isentropic relation, and the total energy per unit volume then follows from Eq. (2-4).

The above scheme, assuming as it does a constant value for the pressure over the whole boundary of the grid, is clearly inconsistent with acoustic radiation to the farfield. It is this portion of NASPROP-E which had to be modified for the present application. First, the shape of the outer boundary in physical space was changed from the hemisphere-cylinder combination described in the last paragraph, to the fully cylindrical shape shown in Fig. 1. Although the matching to the outer flow solution can in principle be accomplished for an arbitrarily shaped interface, for reasons which will become clearer in Section 3 it is much easier if each portion of the interface is parallel to one of the coordinate directions. We are indebted to Drs. L. Bober and H. Huynh of NASA Lewis who made the necessary mesh alterations for us and stored the new grid on their CRAY system where we could directly access it. It should be noted that this change involves only the mesh generation program, and is essentially transparent to the three-dimensional flowfield program.

Changes have also been made within the flowfield program to allow for a variable pressure distribution on the interface. As explained in Sections 3 and 4, NASPROP-E is used to compute  $\partial p / \partial n$  on the interface, which is used by the BIE package to compute a new p distribution there. This new information must somehow then be used as an updated outer boundary condition for the next iteration through NASPROP-E; this is complicated by the fact that p is not one of the primary variables stored in the solution vector Q, cf. Eq. (2-3). Accordingly, at the upstream vertical face and the cylindrical sidewall in Fig. 1 the updated pressure from BIE is used in Eq. (2-4) to compute and store new total energy values on the interface, assuming the velocity components retain their free-stream values. On the downstream vertical face, where, u, v and w vary significantly, the same MOC method is still used to set new values for the

velocities, density and energy. However, now the p values from BIE are used as input rather than  $p_\infty$ .

This completes the discussion of the NASPROP-E portion of the code. The next section discusses in detail the theory behind its interaction with the BIE solution of the outer flow.

### Section 3

#### MATCHING ACROSS THE INTERFACE

The preceding section gave an overview of how the NASPROP-E code solves the nonlinear Euler equations in the inner flow region, and what changes were necessary to allow it to accept arbitrary outer pressure boundary conditions from the BIE package. This section discusses in more detail the theory behind how the two codes were intended to interact. There were three major incompatibilities between the codes which had to be addressed: NASPROP-E originally used a hemisphere/cylinder outer boundary, while BIE was designed with a fully cylindrical inner boundary in mind; NASPROP-E works in blade-fixed coordinates whereas the coordinate system in BIE does not rotate; NASPROP-E allows for a uniform subsonic axial flow, while the classical acoustic analysis in BIE does not. The first of these was easily resolved by switching to a cylindrical outer boundary in NASPROP-E, as described in Section 2. As will be seen shortly, this also facilitates transfer of the boundary conditions between the two. Resolution of the remaining incompatibilities is described below.

#### Evaluation of Normal Pressure Gradient at Interface

Figure 2 is a sketch of the same cylindrical interface shown in Fig. 1, but here with emphasis on the outer flow region.  $S_A$  refers to the upstream vertical face at axial location  $z_u$ ,  $S_B$  to the cylindrical sidewall of radius  $R_S$ , and  $S_C$  to the downstream vertical face at  $z_d$ ; the total ensemble is denoted by  $S$ . Keep in mind that  $S$  is a fictitious surface sufficiently far removed from the propeller, several blade diameters say, so that nonlinear effects such as shock waves are assumed to be negligible.

We have the choice of using NASPROP-E to specify  $\partial p / \partial n$  on  $S$  and then using BIE to get  $p$ , or using NASPROP-E to specify  $p$  on  $S$  and using BIE to determine  $\partial p / \partial n$ . Due to the way in which the outer boundary conditions are set in NASPROP-E (cf. Section 2), the first alternative is clearly preferable. We thus need to evaluate the outward normal pressure gradient in the blade-fixed  $(z, r, \phi)$  frame in terms of the solution computed in the boundary-conforming  $(\xi, \eta, \zeta)$  coordinates. Using the chain rule for differentiation on surface  $S_A$  we have

$$\partial p / \partial n = -p_z = -(\xi_z p_\xi + \eta_z p_\eta + \zeta_z p_\zeta) \quad (3-1a)$$

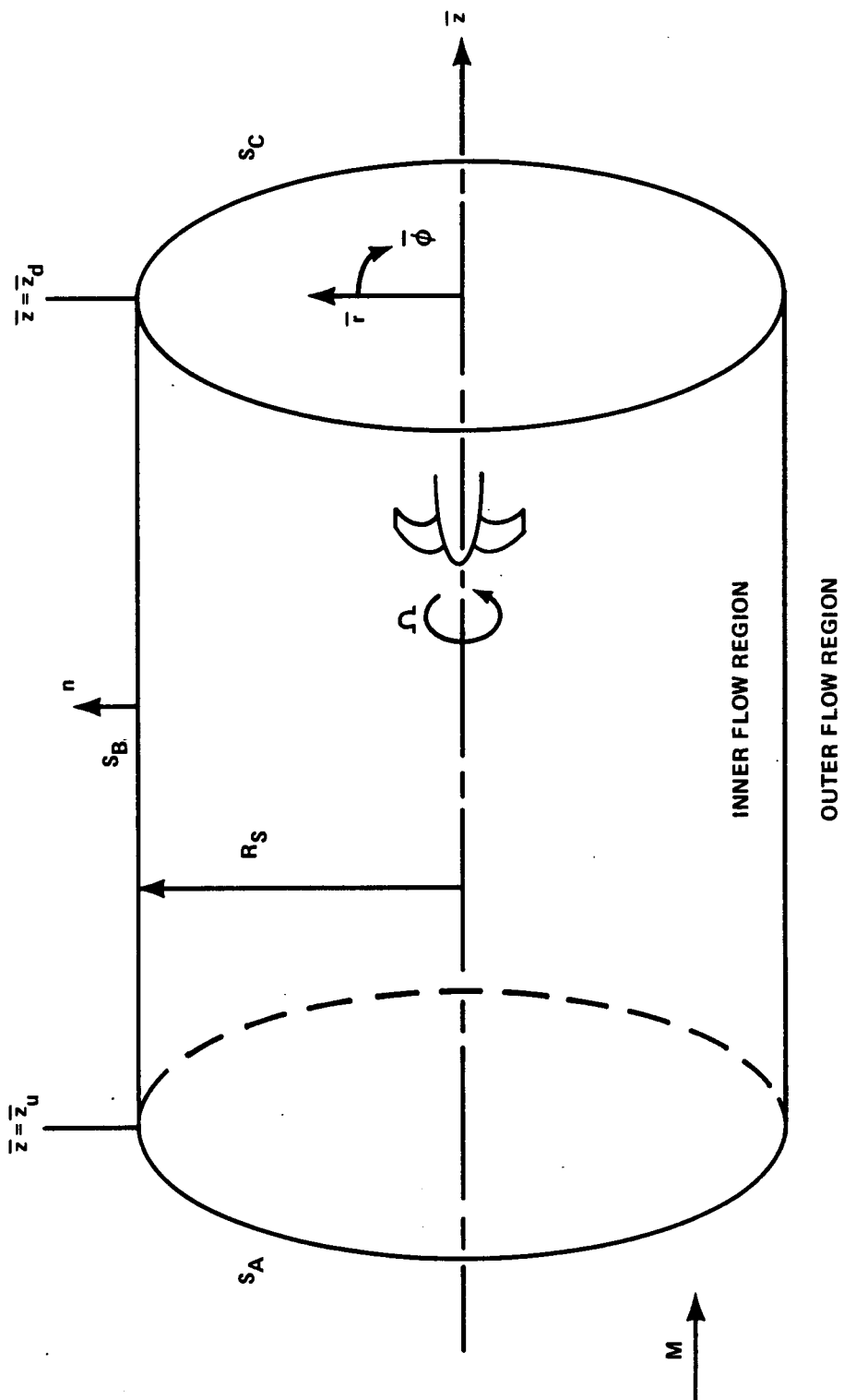


Figure 2. INTERFACE SURFACE S ACROSS WHICH INNER AND OUTER FLOW SOLUTIONS ARE MATCHED (not to scale)

while on  $S_B$ ,

$$\partial p / \partial n = p_r = \xi_r p_\xi + \eta_r p_\eta + \zeta_r p_\zeta \quad (3-1b)$$

and on  $S_C$ ,

$$\partial p / \partial n = p_z = \xi_z p_\xi + \eta_z p_\eta + \zeta_z p_\zeta \quad (3-1c)$$

The metrics  $\xi_z, \xi_r$  etc. are already stored (cf. Eq. (2-9)). Evaluation of the pressure gradients on the right is a two-step process. First the pressures at grid points on and near S are evaluated for the stored solution vector Q using Eq. (2-4). Then standard second-order accurate difference formulae are applied to get  $p_\xi, p_\eta$  and  $p_\zeta$ .

Equations (3-1) define the normal pressure gradient only within the pie-shaped sector formed by one blade passage, say  $0 \leq r \leq R_s$  and  $0 \leq \phi \leq 2\pi/B$ . Because all the blades are identical, this pattern will repeat itself B times around the axis in both hub-fixed and blade-fixed coordinates. It is natural then to represent the variation as a Fourier series:

$$\partial p(z_u, r, \phi) / \partial n = A_0^n(r) + 2 \operatorname{Re} \sum_{m=1}^{\infty} A_m^n(r) e^{imB\phi} \quad (3-2a)$$

$$\partial p(z, R_s, \phi) / \partial n = B_0^n(z) + 2 \operatorname{Re} \sum_{m=1}^{\infty} B_m^n(z) e^{imB\phi} \quad (3-2b)$$

$$\partial p(z_d, r, \phi) / \partial n = C_0^n(r) + 2 \operatorname{Re} \sum_{m=1}^{\infty} C_m^n(r) e^{imB\phi} \quad (3-2c)$$

where the coefficients are found, using Eq. (3-1) as input, from

$$A_m^n = \frac{B}{2\pi} \int_0^{2\pi/B} \frac{\partial p(z_u, r, \phi)}{\partial n} e^{-imB\phi} d\phi \quad (3-3a)$$

$$B_m^n = \frac{B}{2\pi} \int_0^{2\pi/B} \frac{\partial p(z, R_s, \phi)}{\partial n} e^{-imB\phi} d\phi \quad (3-3b)$$

$$C_m^n = \frac{B}{2\pi} \int_0^{2\pi/B} \frac{\partial p(z_d, r, \phi)}{\partial n} e^{-imB\phi} d\phi \quad (3-3c)$$

The above forms apply to surfaces  $S_A$ ,  $S_B$  and  $S_C$  respectively. For later reference we also quote here the analogous expansions for the pressure itself:

$$p(z_u, r, \phi) = A_0(r) + 2 \operatorname{Re} \sum_{m=1}^{\infty} A_m(r) e^{imB\phi} \quad (3-4a)$$

$$p(z, R_s, \phi) = B_0(z) + 2 \operatorname{Re} \sum_{m=1}^{\infty} B_m(z) e^{imB\phi} \quad (3-4b)$$

$$p(z_d, r, \phi) = C_0(r) + 2 \operatorname{Re} \sum_{m=1}^{\infty} C_m(r) e^{imB\phi} \quad (3-4c)$$

where

$$A_m(r) = \frac{B}{2\pi} \int_0^{2\pi/B} p(z_u, r, \phi) e^{-imB\phi} d\phi \quad (3-5a)$$

$$B_m(r) = \frac{B}{2\pi} \int_0^{2\pi/B} p(z, R_s, \phi) e^{-imB\phi} d\phi \quad (3-5b)$$

$$C_m(r) = \frac{B}{2\pi} \int_0^{2\pi/B} p(z_d, r, \phi) e^{-imB\phi} d\phi \quad (3-5c)$$

Note that the subscript  $m$  on the coefficients is the Fourier index, while the absence or presence of the superscript  $n$  indicates a coefficient of either the pressure itself or its normal derivative.

Equations (3-2) and (3-4) are written in a blade-fixed frame. The transformation to coordinates  $(\bar{z}, \bar{r}, \bar{\phi})$  which translate with the hub but do not rotate is simply

$$\bar{z} = z \quad \bar{r} = r \quad \bar{\phi} = \phi - \Omega t \quad (3-6)$$

for a propeller rotating in the  $-\bar{\phi}$  direction (as assumed by NASPROP-E) with constant angular velocity  $\Omega$ . When applied to Eq. (3-2) the result is

$$\partial p(\bar{z}_u, \bar{r}, \bar{\phi}, t) / \partial n = A_0^n(\bar{r}) + 2 \operatorname{Re} \sum_{m=1}^{\infty} A_m^n(\bar{r}) e^{imB(\bar{\phi} + \Omega t)} \quad (3-7a)$$

$$\partial p(\bar{z}, R_s, \bar{\phi}, t) / \partial n = B_0^n(\bar{r}) + 2 \operatorname{Re} \sum_{m=1}^{\infty} B_m^n(\bar{z}) e^{imB(\bar{\phi} + \Omega t)} \quad (3-7b)$$

$$\partial p(\bar{z}_d, \bar{r}, \bar{\phi}, t) / \partial n = C_0^n(\bar{r}) + 2 \operatorname{Re} \sum_{m=1}^{\infty} C_m^n(\bar{z}) e^{imB(\bar{\phi} + \Omega t)} \quad (3-7c)$$

and similarly for Eq. (3-4). This clearly shows that the disturbance field on S, and by inference the entire field external to S, consists of a steady component plus a time variation at the Blade Passage Frequency,  $B\Omega$ , and its harmonics.

#### Transformation from Mean Flow to Static Flow

So far our attention has focussed on the boundary conditions to be applied to the outer flow at the interface S. We now consider the equations to be satisfied in this region, where nonlinear effects are assumed negligible. The linearized equations governing the outer flow including the effects of a subsonic axial Mach number, M, can be reduced to a single equation for the pressure,

$$\beta^2 p_{\bar{z}\bar{z}} + \bar{r}^{-1} (\bar{r} p_{\bar{r}})_{\bar{r}} + \bar{r}^{-2} p_{\bar{\phi}\bar{\phi}} - 2M p_{\bar{z}\bar{t}} / a_\infty - p_{\bar{t}\bar{t}} / a_\infty^2 = 0 \quad (3-8)$$

where  $\beta^2 = 1 - M^2$ , and subscripts indicate differentiation. This relation, written in the same hub-fixed coordinates as Eq. (3-7), is the convective form of the wave equation. As noted earlier, the BIE program is designed to work for the equations of classical acoustics with no mean flow. Setting  $M = 0$  in Eq. (3-8), and further assuming a harmonic time dependence with frequency  $\omega = m B \Omega$  in accordance with Eq. (3-7), we get

$$p_{\bar{z}\bar{z}} + \bar{r}^{-1} (\bar{r} p_{\bar{r}})_{\bar{r}} + \bar{r}^{-2} p_{\bar{\phi}\bar{\phi}} + k_m^2 p = 0 \quad (3-9)$$

which is the classic Helmholtz equation solved by BIE,  $k_m$  being the wavenumber of the mth harmonic,  $m B \Omega / a_\infty$ .

Consider the following transformation of both independent and dependent variables (Refs. 10, 11):

$$\bar{r} = \bar{r} \quad \bar{\phi} = \bar{\phi} \quad \bar{z} = \bar{z} / \beta \quad (3-10a)$$

$$\tilde{p} = p \exp(-i M k_m \bar{z} / \beta) \quad (3-10b)$$

Applying this to Eq. (3-8) and cancelling common factors yields

$$\tilde{p}_{\bar{z}\bar{z}} + \bar{r}^{-1} (\bar{r} \tilde{p}_{\bar{r}})_{\bar{r}} + \bar{r}^{-2} \tilde{p}_{\bar{\phi}\bar{\phi}} + (k_m / \beta)^2 \tilde{p} = 0 \quad (3-11)$$

Hence if we identify

$$\tilde{k}_m = k_m / \beta \quad (3-10c)$$

as part of the transformation, we recover the classic Helmholtz equation, (3-9). Thus we have transformed from a convective flow equation in  $(\bar{z}, \bar{r}, \bar{\phi}, \rho)$  space to an analogous static flow equation in  $(\tilde{z}, \tilde{r}, \tilde{\phi}, \tilde{\rho})$  space. An integral formulation can be used to solve the latter problem directly as follows.

Briefly, the solution to Eq. (3-11) in the outer flow in Fig. 2 is uniquely determined by conditions on S and at infinity (outgoing waves only). Let  $\mathcal{L}$  denote the operator on the left-hand side, and G denote the Green's function satisfying the analogous inhomogeneous equation,

$$\mathcal{L}G(\tilde{k}_m, \tilde{x}, \tilde{x}_0) = -\delta(\tilde{x} - \tilde{x}_0) \quad (3-12)$$

where  $\delta$  is the Dirac delta function and  $\tilde{x}_0$  and  $\tilde{x}$  are generic symbols for the vector coordinates of the source and field points in  $(\tilde{z}, \tilde{r}, \tilde{\phi})$  space, respectively. As derived in any standard text on mathematical physics, e.g. Baker and Copson (Ref. 12), the solution to Eq. (3-11) can then be expressed in the following integral form,

$$\tilde{p}(\tilde{x}) = \int_S \left[ G(\tilde{k}_m, \tilde{x}, \tilde{x}_0) \frac{\partial \tilde{p}(\tilde{x}_0)}{\partial \tilde{n}_0} - \tilde{p}(\tilde{x}_0) \frac{\partial G(\tilde{k}_m, \tilde{x}, \tilde{x}_0)}{\partial \tilde{n}_0} \right] d\tilde{\sigma}_0 \quad (3-13)$$

where the integral is over the whole surface  $S(\tilde{x}_0)$  and  $\tilde{n}_0$  denotes the outward normal at the source point  $\tilde{x}_0$  on S. This form assumes only outgoing waves at infinity, and that there are no sources external to S.

If a Green's function G can be found which vanishes on S, Eq. (3-13) reduces to a simple quadrature over p. This corresponds to replacing S by a dipole distribution. Conversely, if  $\partial G / \partial \tilde{n}_0$  can be made to vanish on S, the solution reduces to a quadrature over  $\partial p / \partial \tilde{n}_0$ , corresponding to a monopole representation on S. In general an analytical representation for G with either of these convenient properties is not possible for an arbitrary surface S, including the finite length cylinder used here. In this case it is convenient to use the free-space Green's function; either p or  $\partial p / \partial \tilde{n}_0$  is assumed known on S, and Eq. (3-13) in the limit where  $\tilde{x}$  approaches the surface provides an integral equation for the remaining unknown. The inversion of this

integral equation is the function served by the BIE method described in Section 4. The choice of whether to regard  $p$  or  $\partial p / \partial n$ , as given in the BIE solution is here dictated by how easily the solved quantity could be incorporated in the outer boundary condition of NASPROP-E. From the discussion toward the end of Section 2, it is clear that  $\partial p / \partial n$  would be difficult to enforce as a boundary condition on the inner flow. So we have chosen to have  $\partial p / \partial n$  specified by the finite difference solution, as anticipated by Eqs. (3-1) through (3-7).

It remains to be seen how the transformation in Eq. (3-10) affects the boundary conditions. First we note that the radius of the cylindrical interface  $S$  is unchanged by (3-10a), but its length is increased by the factor  $\beta^{-1}$ . The wavenumber of each harmonic of the acoustic field is also increased by this factor. Further, BIE will need as input not the  $\partial p / \partial n$  specified in Eq. (3-7), but rather  $\partial \tilde{p} / \partial \tilde{n}$  in the transformed space. Differentiation of Eq. (3-10b) yields the following relation between the two:

$$\frac{\partial \tilde{p}}{\partial \tilde{n}} = \left[ \frac{\partial p}{\partial n} \frac{\partial n}{\partial \tilde{n}} - i \frac{Mk_m}{\beta} p \frac{\partial \tilde{z}}{\partial \tilde{n}} \right] e^{-\frac{iMk_m}{\beta} \tilde{z}} \quad (3-14)$$

Thus we see that in order to specify  $\partial \tilde{p} / \partial \tilde{n}$  in the transformed space, in general both the pressure and its normal derivative must be supplied in physical space. Note that on  $S_A$  and  $S_C$ ,

$$\frac{\partial n}{\partial \tilde{n}} = \frac{\partial z}{\partial \tilde{z}} = \beta \qquad \frac{\partial \tilde{z}}{\partial \tilde{n}} = \mp 1$$

while on  $S_B$ ,

$$\frac{\partial n}{\partial \tilde{n}} = \frac{\partial r}{\partial \tilde{r}} = 1 \qquad \frac{\partial \tilde{z}}{\partial \tilde{n}} = 0$$

so that Eq. (3-14) specializes to

$$\frac{\partial \tilde{p}}{\partial \tilde{n}} = \left[ \beta \frac{\partial p}{\partial n} + i \frac{Mk_m}{\beta} p \right] e^{-\frac{iMk_m}{\beta^2} z_u} \quad (3-15a)$$

$$\frac{\partial \tilde{p}}{\partial \tilde{n}} = \frac{\partial p}{\partial n} e^{i \frac{Mk_m}{\beta^2} z} \quad (3-15b)$$

$$\frac{\partial \tilde{p}}{\partial \tilde{n}} = \left[ \beta \frac{\partial p}{\partial n} - i \frac{Mk_m}{\beta} p \right] e^{-\frac{iMk_m}{\beta^2} z_d} \quad (3-15c)$$

on surfaces  $S_A$ ,  $S_B$  and  $S_C$  respectively. Had an arbitrary curvilinear interface been used, the evaluation of Eq. (3-14) would not have been so simple; it was for this reason that the cylindrical shape was chosen. It follows from Eq. (3-15) that the Fourier coefficients of  $\partial\tilde{p}/\partial\tilde{n}$  are related to those for  $p$  and  $\partial p/\partial n$  (cf. Eqs. (3-2) through (3-7)) by:

$$\tilde{A}_m^n(\tilde{r}) = \left[ \beta A_m^n(r) + i \frac{Mk_m}{\beta} A_m(r) \right] e^{-\frac{iMk_m}{\beta^2} z_u} \quad (3-16a)$$

$$\tilde{B}_m^n(\tilde{z}) = B_m^n(z) e^{-\frac{iMk_m}{\beta^2} z} \quad (3-16b)$$

$$\tilde{C}_m^n(\tilde{r}) = \left[ \beta C_m^n(r) - i \frac{Mk_m}{\beta} C_m(r) \right] e^{-\frac{iMk_m}{\beta^2} z_d} \quad (3-16c)$$

which again apply to  $S_A$ ,  $S_B$  and  $S_C$  respectively. Note that when evaluating the above for  $m = 0$ ,  $k_m = 0$ .

It is the Fourier coefficients defined by Eq. (3-16) which are actually passed to the BIE package as a representation of  $\partial\tilde{p}/\partial\tilde{n}$  over  $S$ . BIE then inverts the integral equation derived from (3-13), as discussed in Section 4, for the transformed pressure  $\tilde{p}$  on  $S$ . Actually, BIE must do an independent calculation for each harmonic, as the constant  $\tilde{k}_m$  in Eq. (3-13) will be different for each value of  $m$ . It returns a set of Fourier coefficients  $\tilde{A}_m$ ,  $\tilde{B}_m$  and  $\tilde{C}_m$  representing the variation of  $\tilde{p}$  over  $S_A$ ,  $S_B$  and  $S_C$  in the transformed plane. These coefficients are converted to their counterparts in physical, blade-fixed coordinates through Eq. (3-10b), giving:

$$A_m(r) = \tilde{A}_m(\tilde{r}) e^{+\frac{iMk_m}{\beta} \tilde{z}_u} \quad (3-17a)$$

$$B_m(z) = \tilde{B}_m(\tilde{z}) e^{+\frac{iMk_m}{\beta} \tilde{z}} \quad (3-17b)$$

$$C_m(r) = \tilde{C}_m(\tilde{r}) e^{+\frac{iMk_m}{\beta} \tilde{z}_d} \quad (3-17c)$$

When substituted into Eq. (3-4) these define a new pressure distribution over the surface  $S$ .

## Update to Boundary Conditions

The new pressure distribution found by BIE in general will not match that used as the boundary condition on the nonlinear flow equations solved by NASPROP-E. The disparity is used to update the boundary conditions used for the next time step as follows. Let  $p_i^q$  denote the pressure distribution on S used as the boundary condition on the inner flow at the qth time step. This solution is used as input to the BIE package, as per the procedure described above, to determine the pressure over the same surface based on the outer linearized equations,  $p_o^q$  say. The boundary conditions on NASPROP-E for the next time step are then updated as follows:

$$\begin{aligned} p_i^{q+1} &= p_i^q + \alpha (p_o^q - p_i^q) \\ &= \alpha p_o^q + (1-\alpha) p_i^q \end{aligned} \quad (3-18)$$

The parameter  $\alpha$ , where  $0 < \alpha \leq 1$ , has been introduced to allow for underrelaxation of the iterations. This was found necessary for convergence of a similar iterative process used at Calspan in our studies of adaptive-wall wind tunnels (Ref. 13). As noted at the end of Section 2, p is not one of the primary variables used by NASPROP-E. Therefore, on  $S_A$  and  $S_B$  the new values from Eq. (3-18) are used to recompute the local total energy at the boundary grid points using Eq. (2-4). On surface  $S_C$ , the Method of Characteristics (MOC) is used to update the boundary values for density, velocity, and energy using the new pressures.

Eventually, the above iterative process should converge in the sense that the discrepancy between  $p_i^q$  and  $p_o^q$  grows progressively smaller. Convergence is evaluated in CALPROP by testing whether

$$\left[ \frac{1}{N_T} \sum (p_i^q - p_o^q)^2 \right]^{\frac{1}{2}} \leq \epsilon \ll 1 \quad (3-19)$$

where the sum is over the total number,  $N_T = JMAX + KMAX - 1$ , of grid points on S, and  $\epsilon$  is set by the user. When Eq. (3-19) is satisfied, the composite solution provided by NASPROP-E and BIE should consistently satisfy the blade boundary conditions, the free-field radiation conditions, and match p and  $\partial p / \partial n$  across the interface S.

The above procedure for interfacing between NASPROP-E and BIE is summarized briefly in Section 5 as a means of introducing the new routines in

the combined code CALPROP. This recapitulation makes clearer the sequence in which each of the operations is performed.

After convergence the acoustic near-field can be evaluated by interpolation in the finite-difference grid. The acoustic far-field is easily evaluated from Eq. (3-13), which now becomes a simple quadrature over the known  $\tilde{p}$  and  $\partial\tilde{p}/\partial n$  distributions. This is also done in BIE, which is described in more detail in the next section.

Section 4  
OUTER LINEARIZED ACOUSTIC MODEL

Review of the BIE Method

A solution technique utilizing a discretized surface integral is commonly referred to as a Boundary Integral Equation (BIE) method. The outstanding feature of this method is that the dimension of the problem is reduced by one, since only the boundary (surface) of the body is dealt with. Thus, the BIE method is particularly suited for field problems involving an infinite domain or a finite domain in which the field variables are needed at only a few points. The BIE has been used successfully in solving problems governed by linear elliptic, parabolic, and hyperbolic partial differential equations (Ref. 14). Recently, Shaw (Ref. 15) has given an excellent review of the application of the BIE to wave problems.

In principle, the BIE formulation can be derived from Green's theorem (Ref. 12, 16, 17) which relates the surface integral over  $S$  to the volume integral over  $V$  bounded by  $S$  for any two functions  $p$  and  $\psi$  sufficiently smooth and nonsingular in  $V$ :

$$\int_S \left( p \frac{\partial \psi}{\partial n} - \psi \frac{\partial p}{\partial n} \right) dS = \int_V \left( p \nabla^2 \psi - \psi \nabla^2 p \right) dV \quad (4-1)$$

where  $n$  is the outward normal of  $S$  (i.e.,  $n$  is directed out of the region  $V$ ).

We apply this identity to three-dimensional acoustic problems, e.g., sound radiation from a vibrating body of surface area  $S_0$ , using the freespace Green's function  $\exp(-ikR)/R = \psi$  and the acoustic pressure  $p$ , where  $R$  is the distance between any two points  $P$  and  $Q$  in  $V$ , and  $k$  is the wave number. This problem is classified as an exterior problem governed by Helmholtz's equation where all physical quantities are defined outside of the body  $S_0$ . The volume  $V$  is the space bounded by  $S_0$  and the surface  $\Sigma$  at infinity. The surface at infinity can be represented by a sphere of infinite radius. The acoustic pressure  $p$  is smooth and nonsingular, but  $\psi$  is singular when  $P = Q$ . To remove this singularity, we exclude a portion of  $V$  in a small sphere  $\sigma$  of radius  $\epsilon$  surrounding  $P$  as shown in Fig. 3. Now, since  $P \neq Q$ , both  $\psi$  and  $p$  satisfy the Helmholtz equation  $\nabla^2 \psi + k^2 \psi = 0$  and  $\nabla^2 p + k^2 p = 0$  in  $V$ , the volume integral in Eq. (4-1) is 0:

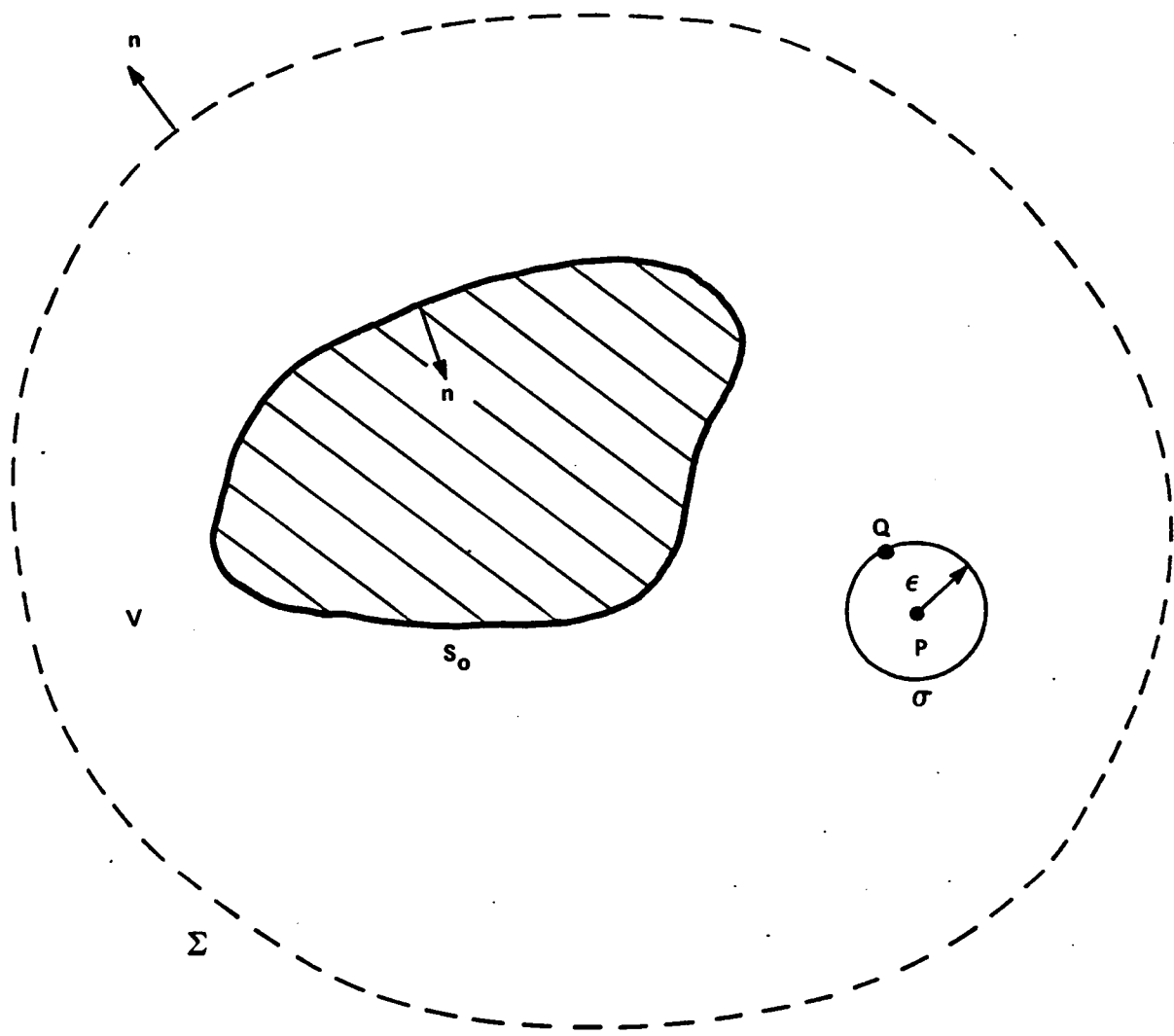


Figure 3 RADIATION FROM A SURFACE  $S_0$  INTO AN EXTERIOR REGION  $V$

$$\int_{S_0 + \sigma + \Sigma} \left( p \frac{\partial \psi}{\partial n} - \psi \frac{\partial p}{\partial n} \right) dS = 0. \quad (4-2)$$

Taking the limit as  $\epsilon$  tends to zero for the integral over  $\sigma$

$$\begin{aligned} & \int \left( p \frac{\partial \psi}{\partial n} - \psi \frac{\partial p}{\partial n} \right) dS \\ &= \lim_{R=\epsilon=0} \int_{\sigma} \left[ p \frac{\partial}{\partial n} \left( \frac{e^{-ikR}}{R} \right) - \frac{e^{-ikR}}{R} \frac{\partial p}{\partial n} \right] dS = 4\pi p(P) \end{aligned} \quad (4-3)$$

which results from using a spherical coordinate system centered at P and the fact that  $\partial/\partial n = -\partial/\partial R$  where  $p(P)$  is the acoustic pressure at P. The surface integral over the portion of S at infinity, i.e.,  $\Sigma$ , is zero because of the Sommerfeld radiation condition. Defining a new normal  $\nu = -n$  directed outward from the body (i.e., into V), then Eq. (4-2) becomes

$$\int_{S_0} \left[ p \frac{\partial}{\partial \nu} \left( \frac{e^{-ikR}}{R} \right) - \frac{e^{-ikR}}{R} \frac{\partial p}{\partial \nu} \right] dS_0 = 4\pi p(P). \quad (4-4)$$

Now consider Q as a source point on the surface  $S_0$  and allow the field point P to approach  $S_0$ . Providing that the surface  $S_0$  has a unique tangent at Q, the singularity that occurs as  $Q = P$  may be removed by excluding the portion of V in a small hemisphere  $\sigma$  around P. Following the same procedure used in deriving Eq. (4-4), the following result is obtained:

$$\int_{S_0} \left[ p \frac{\partial}{\partial \nu} \left( \frac{e^{-ikR}}{R} \right) - \frac{e^{-ikR}}{R} \frac{\partial p}{\partial \nu} \right] dS_0 = 2\pi p(P). \quad (4-5)$$

Equation (4-5) is called the Surface Helmholtz Integral Equation.

If the field point P is inside the body, then  $\psi$  and  $p$  are always nonsingular in V. Therefore Eq. (4-1) yields, for this case,

$$\int_{S_0} \left[ p \frac{\partial}{\partial \nu} \left( \frac{e^{-ikR}}{R} \right) - \frac{e^{-ikR}}{R} \frac{\partial p}{\partial \nu} \right] dS_0 = 0 \quad (4-6)$$

which is called the Interior Helmholtz Integral Equation. Equations (4-4) through (4-6) can be written in a compact form:

$$\int_{S_0} \left[ p \frac{\partial}{\partial \nu} \left( \frac{e^{-ikR}}{R} \right) - \frac{e^{-ikR}}{R} \frac{\partial p}{\partial \nu} \right] dS_0 = C(P) p(P) \quad (4-7)$$

where

$$\begin{aligned} C(P) &= 4\pi \quad \text{for the field points outside the body,} \\ &= 2\pi \quad \text{for the field points on the surface of the body,} \\ &= 0 \quad \text{for field points inside the body.} \end{aligned}$$

As mentioned before, for field points on the surface  $S_0$ ,  $C(P) = 2\pi$  only when the surface has a unique tangent at  $P$ . A more general expression for  $C(P)$  is necessary if there is no unique tangent plane at  $P$ , i.e., when  $P$  is at a corner or edge of  $S_0$ . For this more general expression, note first that the counterpart of Eq. (4-7) for a function  $U$  satisfying Laplace's equation inside the region bounded by  $S_0$  has the form

$$\int_{S_0} \left[ \frac{1}{R} \frac{\partial U}{\partial \nu} - U \frac{\partial}{\partial \nu} \left( \frac{1}{R} \right) \right] dS_0 = C^0(P) U(P) \quad (4-8)$$

in which  $(1/R)$  is the counterpart of  $\exp(-ikR)/R$  for the Laplace operator, and  $C^0(P)$  is the result of the limit of the integrals over a small "bubble-like" region  $\sigma$  with "base" centered at  $P$  similar to the hemisphere mentioned earlier. However for  $P$  at an edge or corner, the bubble-like region is not a hemisphere and the base is not flat in the limit. The required result can be obtained from Eq. (4-8) using  $U = 1$  which gives

$$C^0(P) = - \int_{S_0} \frac{\partial}{\partial \nu} \left( \frac{1}{R} \right) dS_0 \quad (4-9)$$

which has the interpretation of the inner solid angle at  $P$ . Since the limit processes depend only on the order of singularity of  $\psi$  which is the same for both the Laplace and Helmholtz operators, and since  $C(P)$  in Eq. (4-7) may be obtained in the limit as  $P$  approaches  $S_0$  from outside  $S_0$ ,  $C(P)$  has the interpretation of the outer solid angle at  $P$  so that

$$C(P) + C^{\circ}(P) = 4\pi. \quad (4-10)$$

Thus,  $C(P) = 4\pi - C^{\circ}(P)$  and Eq. (4-5) can be rewritten:

$$\int_{S_0} \left[ p \frac{\partial}{\partial \nu} \left( \frac{e^{-ikR}}{R} \right) - \left( \frac{e^{-ikR}}{R} \right) \frac{\partial p}{\partial \nu} \right] dS_0 = \left[ 4\pi + \int_{S_0} \frac{\partial}{\partial \nu} \left( \frac{1}{R} \right) dS_0 \right] p(P). \quad (4-11)$$

Equation (4-11) is a general Surface Helmholtz Integral Equation applicable to any arbitrary surface.

### Axisymmetric Formulation

When the surface is a body of revolution (Fig. 4) then

$$dS_0 = \rho(Q) d\phi dL_0(Q)$$

where  $dL_0$  is the differential length of the generator of the body. We now rename our normal  $\nu$  to  $n$  to conform with convention in acoustics. Further, if we expand  $p$  and  $\partial p / \partial n$  on  $S_0$  into Fourier series in the  $\phi$  direction:

$$p(Q) = \sum_m A_m e^{imB\phi}$$

$$\frac{\partial p}{\partial n}(Q) = \sum_m A_m^n e^{imB\phi}$$

where  $B$  (the blade number) is a constant, then Eq. (4-11) may be written for a single harmonic,  $A_m$  and  $A_m^n$ , as

$$\int_{L_0} \left[ A_m \int_0^{2\pi} \frac{\partial \psi}{\partial n} e^{imB\phi} d\phi - A_m^n \int_0^{2\pi} \psi e^{imB\phi} d\phi \right] \rho dL_0 = C(P) A_m(P) \quad (4-12)$$

where  $A_m(P) = A_m e^{imB\phi(P)}$  is the pressure at a field point  $P$ . The axisymmetric formulation above allows us to decouple the integration of Eq. (4-11) into the evaluation of two line integrals in the  $(L_0, \phi)$  coordinate directions, Eq. (4-12). Further, the integrals in the  $\phi$  direction are independent of the boundary data,  $A_m$  and  $A_m^n$ , and can be evaluated without the use of nodes and

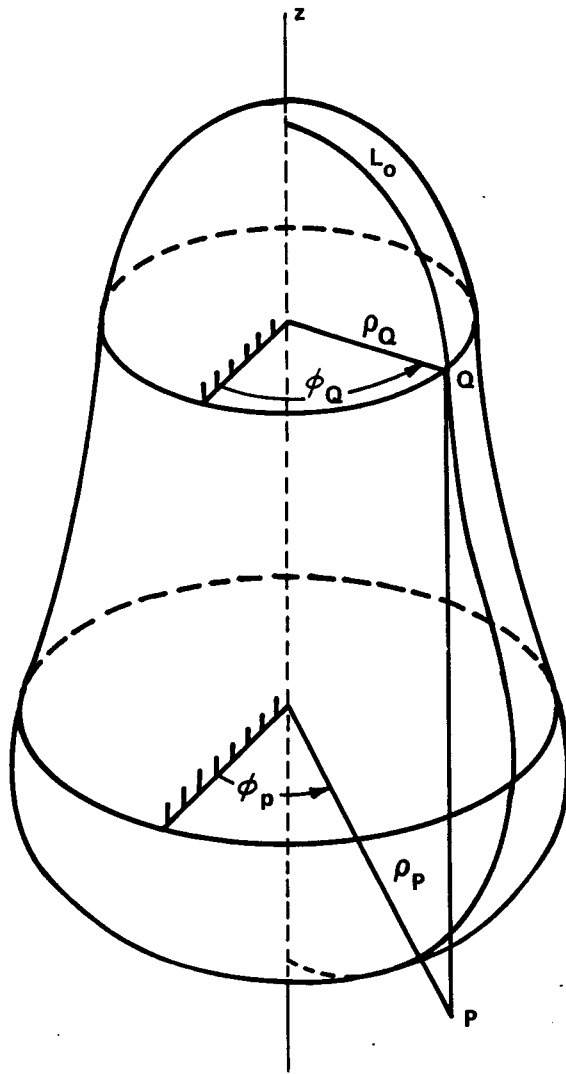


Figure 4 A SIMPLY CONNECTED AXISYMMETRIC BODY

elements. Thus, all element discretization can be confined to the generator of the axisymmetric body, i.e. the elements are now line segments. The boundary data need only be specified at the nodes on the generator.

### Numerical Implementation

Because the exterior solution reduces to a discretization of the generator, only one-dimensional elements (line segments) are needed. The same quadratic interpolation is used for both the geometry and the function variation on each segment (isoparametric elements). The coordinates  $(\rho, z)$  of any point on the generator (see Fig. 4) can be represented as:

$$\rho(\xi) = \sum_{\alpha=1}^3 N_{\alpha}(\xi) \rho_{\alpha} \quad (4-13)$$

$$z(\xi) = \sum_{\alpha=1}^3 N_{\alpha}(\xi) z_{\alpha} \quad (4-14)$$

where  $N_{\alpha}(\xi)$  are the shape (interpolating) functions in the mapped domain  $(-1 \leq \xi \leq 1)$  corresponding to node  $\alpha$  (each element is a line segment consisting of three nodes) and  $(\rho_{\alpha}, z_{\alpha})$  are the physical coordinates of node  $\alpha$ . It is implicit here that all elements are mapped into a "clean" -1 to 1 region. All integrations are carried out in this new region. The  $N_{\alpha}(\xi)$  are

$$\begin{aligned} N_1(\xi) &= -\frac{1}{2}\xi + \frac{1}{2}\xi^2, \\ N_2(\xi) &= 1 - \xi^2, \\ N_3(\xi) &= \frac{1}{2}\xi + \frac{1}{2}\xi^2, \end{aligned} \quad (4-15)$$

where  $\xi$  is the coordinate in the -1 to 1 mapped space.

For an element  $k$ ,  $A_m$  and  $A_m^n$  are represented using the same shape functions, Eq. (4-15):

$$\begin{aligned} A_{mk}(\xi) &= \sum_{\alpha=1}^3 N_{\alpha}(\xi) A_{mk\alpha} \\ A_{mk}^n(\xi) &= \sum_{\alpha=1}^3 N_{\alpha}(\xi) A_{mk\alpha}^n \end{aligned} \quad (4-16)$$

where  $A_{mk\alpha}$  and  $A_{mk\alpha}^n$  are the pressure and normal derivative of the pressure, respectively, at node  $\alpha$  on element  $k$  for harmonic  $m$ . Substituting Eq. (4-16) into Eq. (4-12) yields:

$$\sum_{k=1}^K \left[ \sum_{\alpha=1}^3 A_{mk\alpha} \int_{-1}^1 K_{am}(\xi) N_{\alpha}(\xi) \rho(\xi) J_k(\xi) d\xi \right. \quad (4-17)$$

$$\left. - \sum_{\alpha=1}^3 A_{mk\alpha}^n \int_{-1}^1 K_{bm}(\xi) N_{\alpha}(\xi) \rho(\xi) J_k(\xi) d\xi \right] = C(P) A_m(P) ,$$

where

$$K_{am}(\xi) = \int_0^{2\pi} \frac{\partial \psi}{\partial n} e^{im\phi} d\phi, \quad K_{bm}(\xi) = \int_0^{2\pi} \psi e^{im\phi} d\phi, \quad (4-18)$$

K is the total number of elements on the generator and  $J_k(\xi)$  is the Jacobian of the mapping from  $(\rho, z)$  to  $\xi$ , given by:

$$J_k(\xi) = \left[ \left( \frac{d\rho}{d\xi} \right)^2 + \left( \frac{dz}{d\xi} \right)^2 \right]^{\frac{1}{2}} .$$

In the same manner, the constant C(P) in Eq. (4-17) is given by:

$$C(P) = 4\pi + \sum_{k=1}^K \int_{-1}^1 K_c(\xi) \rho(\xi) J_k(\xi) d\xi, \quad (4-19)$$

where

$$K_c(\xi) = \int_0^{2\pi} \frac{\partial}{\partial n} \left( \frac{1}{R} \right) d\phi. \quad (4-20)$$

If we put P on the surface at a node which we identify as j ( $j = 1$  to L, where L is the total number of elements) then  $A_m(P) = A_{mj}$ , and Eq. (4-17) may be written as

$$\sum_{k=1}^K \sum_{\alpha=1}^3 A_{mk\alpha} a_{mkj}^{\alpha} - A_{mj} \left[ 2 + \sum_{k=1}^K c_{kj}^{\alpha} \right] = \sum_{k=1}^K \sum_{\alpha=1}^3 A_{mk\alpha}^n b_{mkj}^{\alpha}, \quad (4-21)$$

where

$$a_{mkj}^{\alpha} = \frac{1}{2\pi} \int_{-1}^1 K_{am}(\xi) N_{\alpha}(\xi) \rho(\xi) J_k(\xi) d\xi \quad (4-22)$$

$$b_{mkj}^{\alpha} = \frac{1}{2\pi} \int_{-1}^1 K_{bm}(\xi) N_{\alpha}(\xi) \rho(\xi) J_k(\xi) d\xi \quad (4-23)$$

$$c_{kj}^{\alpha} = \frac{1}{2\pi} \int_{-1}^1 K_c(\xi) \rho(\xi) J_k(\xi) d\xi \quad (4-24)$$

In the above expressions  $j$  denotes the global node number where  $P$  is located and  $k, \alpha$  denote the element number and local node number, respectively, of the location of  $Q$ . If we let  $\ell$  be the global node number for  $Q$  corresponding to a given  $k, \alpha$  combination, Eq. (4-21) may be written as

$$\sum_{\ell=1}^L A_{m\ell} \hat{a}_{m\ell j} - A_{mj} \left[ 2 + \sum_{k=1}^K c_{kj} \right] = \sum_{\ell=1}^L A_{m\ell}^n b_{m\ell j}, \quad (4-25)$$

or

$$\sum_{\ell=1}^L a_{m\ell j} A_{m\ell} = \sum_{\ell=1}^L b_{m\ell j} A_{m\ell}^n \quad (4-26)$$

where

$$a_{m\ell j} = \hat{a}_{m\ell j} - \left[ 2 + \sum_{k=1}^K c_{kj} \right] \delta_{j\ell}$$

where  $\delta_{j\ell}$  is the Kronecker delta function. Equation (4-26) may be written in matrix form as:

$$[a_m] \{A_m\} = [b_m] \{A_m^n\} \quad (4-27)$$

If the normal derivative of the acoustic pressure,  $\{A_m^n\}$ , is specified on the surface, then from Eq. (4-27) we may calculate the acoustic pressure  $\{A_m\}$ .

### Calculation of Farfield Sound Pressure

After  $A_m$  has been determined we may determine the sound pressure at an exterior point  $P$  using Eq. (4-12), or its numerical counterpart, Eq. (4-17), with  $C(P) = 4\pi$ . This is a simple quadrature process since (now) both  $A_m$  and  $A_m^n$  are known on the surface.

### The Interior Eigenfrequency Problem

It has long been recognized (Ref. 18) that integral equations of the type given in Eq. (4-12) will not yield a unique solution at certain characteristic frequencies associated with the shape of  $S_0$ . These characteristic frequencies are the eigenfrequencies of the interior of  $S_0$  with an "altered" boundary condition. That is, if we are solving Eq. (4-12) by specifying  $\partial p / \partial n$  on  $S_0$ , then the characteristic frequencies where the nonuniqueness problem arises are the eigenfrequencies of the interior of  $S_0$  determined by setting  $p = 0$  on  $S_0$ . For a cylinder these frequencies are (Ref. 17, p. 429):

$$k_{m\alpha n} = [(n\pi/L)^2 + (\gamma_{m\alpha}/R)^2]^{\frac{1}{2}}, \quad (4-28)$$

where:  $n, \alpha = 1, 2, 3, \dots$ ;  $m = 0, 1, 2, \dots$ ;  $R$  and  $L$  are the radius and length of the cylinder, respectively; and  $\gamma_{m\alpha}$  are the zeroes of the  $m$ th order Bessel function.

The modal density (average number of characteristic frequencies per unit frequency) is proportional to  $k^3$ . Even at moderate values of  $k$  the eigenfrequencies are closely spaced. The following table shows the eigenfrequencies between  $19 \leq \tilde{k}R_S \leq 22$  for the CALPROP interface ( $L/R_S = 1.21$ ) for the  $m = 0$  circumferential mode.

$\alpha$	$n$	$k_{0\alpha n}R_S$
2	7	19.00
4	6	19.54
6	3	19.68
5	5	19.79
3	7	20.13
6	4	20.84
1	8	20.91
7	1	21.37
2	8	21.49
5	6	21.58
4	7	21.66
7	2	21.84

It has been observed (Refs. 5, 19 and 20) that symmetric boundary data will select only certain of the eigenfrequencies. Thus, only the eigenfrequencies above would result in nonuniqueness for symmetric ( $m = 0$ ) *ap/an* boundary data; i.e., the  $m = 1, 2, \dots$  eigenfrequencies would not produce nonuniqueness. This is due to the interplay between the coefficient matrix and the right-hand-side vector (Ref. 19) in Eq. (4-27). In the present problem there is symmetry in the circumferential direction due to the blade spacing. Thus for eight blades only the  $m = 8$  modes will cause nonuniqueness problems. However, a calculation using Eq. (4-28) yielded 32 eigenfrequencies in the range  $19 \leq \tilde{k}R_S \leq 22$  for the CALPROP interface.

## Attempts to Circumvent the Eigenfrequency Problem

There is no general and systematic way to handle the nonuniqueness problem. This fact is evidenced by recent papers (e.g. Ref. 19) proposing new ways to achieve a unique solution to Eq. (4-12). However, the most common method (Refs. 18, 21) to handle nonuniqueness is called CHIEF. In CHIEF a least-squares solution is found by overdetermining the system, Eq. (4-27), with additional points interior to  $S_0$  where  $p = 0$ . These additional equations are given by Eq. (4-6).

A second method (Ref. 22) forms a new integral equation from a linear combination of Eq. (4-12) and its normal derivative. The normal derivative of Eq. (4-12) has a nonunique solution at certain characteristic frequencies, but these eigenfrequencies are not the same as those for Eq. (4-12). Thus, a linear combination of Eq. (4-12) and its derivative will have a unique solution for all values of frequency. This method has been used successfully recently with a combination finite element/boundary element solution approach (Ref. 10).

Nonuniqueness of the solution to Eq. (4-12) is manifested as ill-conditioning in the algebraic system, Eq. (4-27). This ill-conditioning reduces the accuracy of the (unique) solution in a frequency band  $\Delta k$  in the neighborhood of the eigenfrequencies. If it were not for this ill-conditioning over  $\Delta k$ , the nonuniqueness problem would be only of academic interest because it is always possible to avoid the eigenfrequencies by a proper choice of frequency. Thus, it is the ill-conditioning that results from nonuniqueness, and not nonuniqueness per se, that produces inaccurate results in solving Eq. (4-27).

The method used in Ref. 22 works when the eigenfrequencies of Eq. (4-12) and its normal derivative are sufficiently spaced so that the  $\Delta k$  do not overlap. When this condition is met ill-conditioning will not occur. However, at higher frequency, e.g.,  $kR > 20$ , it is expected that this method will not yield good results. It was this consideration that led us to pursue the CHIEF method over the method in Ref. 22.

Another method to overcome the fictitious eigenfrequency problem is the Exterior Overdetermination Method (EODM) (Ref. 19). Based on a combination of the Surface and Exterior Helmholtz Integral Equations, EODM uses an iterative approach. The square system of equations obtained from the Surface Helmholtz Equation is overdetermined by additional equations formed by evaluation of the Exterior Helmholtz Integral Equation at selected points outside the body. An approximate impedance function is assumed on the surface of the body to initiate the iterations. The selection of the locations of the exterior points used in the iteration was found to be critical as a result of some numerical experiments we performed using EODM. If the points are too far removed from the body, two adjacent points yield almost the same equation, thus causing severe ill-conditioning. If the points are too close to the surface, it is not possible to have many points for the same reason. The optimal selection of the number of additional points and their locations corresponding to the desired rate of convergence remains unresolved.

Section 5  
PROGRAM CALPROP

Sections 2 through 4 were devoted to the theory and algorithms used in the NASPROP-E and BIE codes and how they were intended to interact in the resulting combined program, CALPROP. This section is concerned more with the mechanics of how all this was implemented. Originally it was envisioned that CALPROP would consist of a new MAIN program and associated I/O which would essentially treat NASPROP-E and BIE as subroutine packages. However, it was soon realized that since NASPROP-E would comprise the majority of the source code, and already contained much of the required I/O structure, it was easiest to build the new program about its existing framework, with BIE incorporated as a package of subroutines. This approach has the added advantage of making CALPROP that much easier to run for previous users of NASPROP-E. Since NASPROP-E has been documented in Refs. 3 and 4, the emphasis here will be only on modifications to existing routines and descriptions of whatever new routines have been added. The source code images are stored on the NASA Lewis CRAY system as PDN = SRCLIB1, and the executable object code as PDN = OBJLIB1; both have ID = FSSPAN. The program takes up approximately 652K words of storage.

The overall structure of program CALPROP is shown in Fig. 5. Although all subroutines in the program are shown, this is not intended to be a detailed flow chart, but merely to display the major interconnections. The starting point was the NASPROP-E version running on NASA Lewis' CRAY computer, which was permitted to us for this work by Dr. L. Bober. Those routines outside the dashed line are native to NASPROP-E. Some of these required changes and are discussed first below. This is followed by a description of the new routines unique to CALPROP, i.e., those inside the dotted line in Fig. 5. Finally, a description of the BIE package is provided.

Changes to NASPROP-E Routines

The only existing NASPROP-E routines which required modification were AIR3D, INPUT, INITIA and BNDRY as follows:

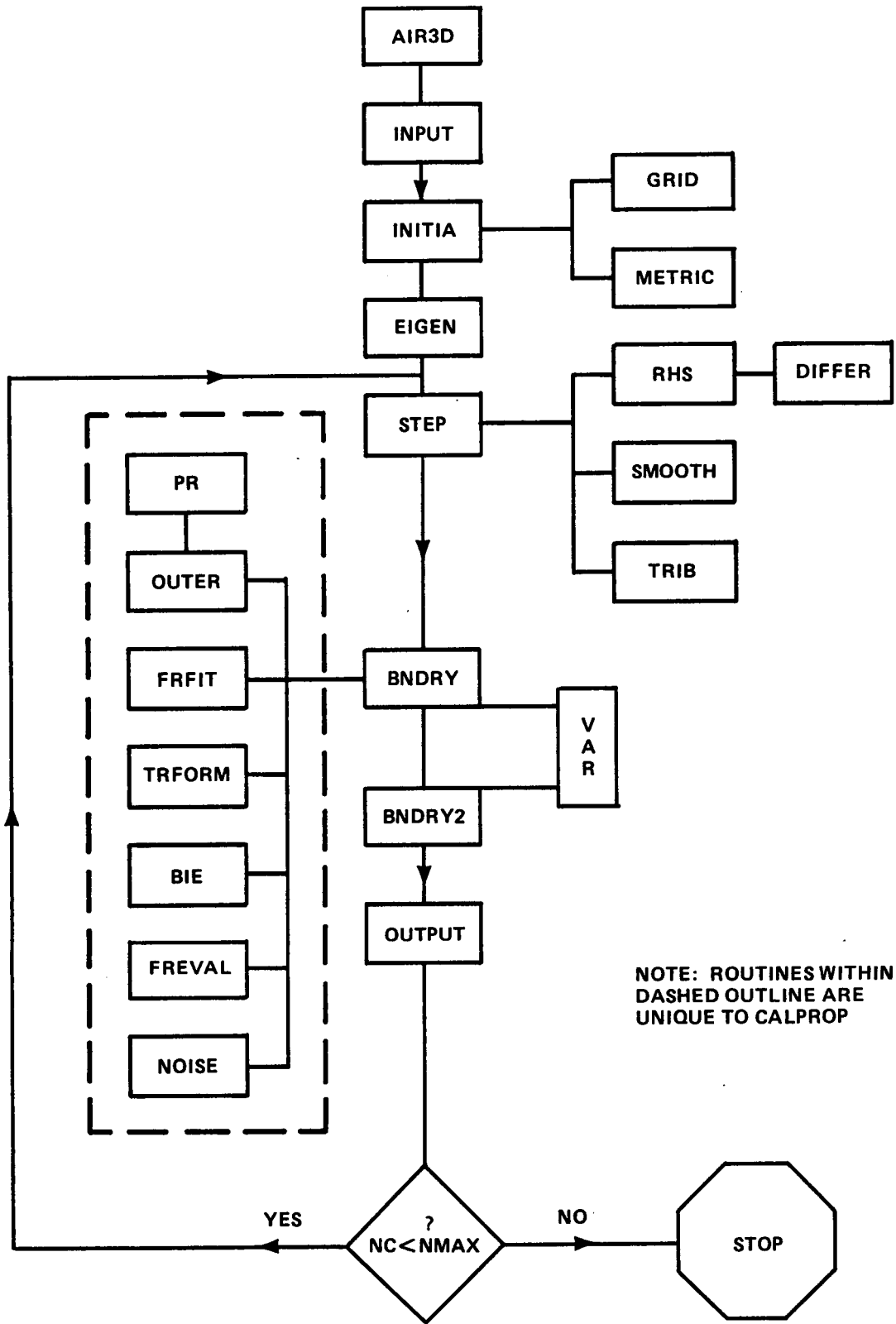


Figure 5. OVERALL STRUCTURE OF CALPROP

AIR3D. This is actually the Main, or driving, program; the only change here is the addition of labelled COMMON/ACOUST/, which is the primary means of transferring data between the NASPROP-E and BIE routines. The variables, in the order which they appear, are defined below.

<u>Variable Name</u>	<u>Description</u>
EPS	Convergence criterion used in Eq. (3-19)
RMS	Left-hand side of Eq. (3-19)
FSBETA	$(1-M^2)^{1/2}$
JA	Value of J grid index at upper left corner of cylindrical grid in Fig. 1
JMPKM	JMAX+KMAX
MMAX	Highest value of harmonic index m, i.e., $0 \leq m \leq MMAX$ , $MMAX \leq 5$
NINT	Integral number of time steps between boundary condition updates using BIE
NSIG	Number of observer positions at which the acoustic signal, SPL, is to be evaluated; $NSIG \leq 20$
RLXBC	Relaxation factor on boundary conditions, $\alpha$ , in Eq. (3-18)
RSIG(IS),ZSIG(IS)	Dimensionless $\bar{r}$ , $\bar{z}$ coordinates of the ISth observer position at which the acoustic signal, SPL, is to be evaluated; normalized by propeller diameter, D; $1 \leq IS \leq NSIG$

<u>Variable Name</u>	<u>Description</u>
SPL(MDUM,IS)	The Sound Pressure Level of the mth harmonic at the ISth observer position, referenced to $p_\infty$ ; MDUM=m+1, $1 \leq MDUM \leq MMAX+1$ , $1 \leq IS \leq NSIG$
WAVK(MDUM)	Dimensionless wavenumber of mth harmonic of acoustic field, $k_m$ , normalized by the reciprocal of propeller diameter
DELPHI, PHASE	Working arrays containing azimuthal grid spacing and phase information used in Fourier decomposition
RTR(I),ZTR(I)	Dimensionless $\tilde{r}$ , $\tilde{z}$ coordinates of Ith grid point on cylindrical interface, $1 \leq I \leq JMAX+KMAX+1$
P(L,I),PN(L,I)	Dimensionless pressure and normal pressure derivative, normalized by $p_\infty$ and $p_\infty /D$ respectively; evaluated at the Ith grid point in the $\tilde{r}$ , $\tilde{z}$ plane and the Lth $\tilde{\phi}$ grid point.
PC(MDUM,I), PNC(MDUM,I)	Dimensionless complex Fourier coefficients of the pressure and its normal derivative, normalized by $p_\infty$ and $p_\infty /D$ respectively; correspond to the mth harmonic, $m=MDUM-1$ , at the Ith grid point in the $\tilde{r}$ , $\tilde{z}$ plane.

Labelled COMMON/ACOUST/ also was added to existing routines INPUT, INITIA, and BNDRY.

INPUT. The principal change here was the addition of new input variables required by CALPROP. The original NASPROP-E would read in 4 input records from TAPE 5 for a start from scratch. In CALPROP, a fifth record is added to read in NINT, MMAX, NSIG and JA with a format 6I5, followed by a sixth record containing EPS and RLXBC with a format 6F10.5. Finally, the coordinate pairs ZSIG(IS), RSIG(IS) for  $IS = 1, NSIG$  are read in using as many input records

as needed with a 6F10.5 format, i.e., 3 pairs to a record. The values for NINT, MMAX, NSIG, JA, EPS and RLXBC are also written on the output file after the other input variables.

INITIA. If  $NINT \leq NMAX$  (cf. discussion of BNDRY below), this routine will now make initialization calls to new routines OUTER and BIE.

BNDRY. There are two routines in NASPROP-E with similar names, BNDRY and BNDRY2. BNDRY2 updates the boundary conditions only on the blade surfaces, and was not changed in any way for CALPROP. BNDRY is responsible for updating the boundary conditions on the nacelle (no changes here), and on the outer surface of the difference grid, i.e. the interface surface S. As mentioned before, this surface was changed from the hemisphere/cylinder shape used in NASPROP-E to a finite length cylinder in  $(z, r, \phi)$  coordinates. This modification only necessitated changes to the mesh generation program which produces the boundary-conforming grid. Hence to BNDRY, which works in the resulting  $(\xi, \eta, \zeta)$  coordinates, this particular change was transparent.

As for updating the outer boundary conditions on S, BNDRY was altered so that how the boundary conditions are handled depends on the relative values of the three parameters NC, NMAX, and NINT. NC is the integral value of the current time step count, and is found in labelled COMMON/COUNT/. NMAX is an input which represents the maximum value of NC to be allowed on this run, and is found in labelled COMMON/BASE/; both are native to NASPROP-E. NINT is the interval, i.e., some integral number of time steps, at which BIE is called to update the boundary conditions. It is an input parameter communicated through labelled COMMON/ACOUST/ (see above), and is new to CALPROP.

Three alternative logic paths are possible. First, if the user specifies his input values such that  $NINT > NMAX$ , BIE is never called, and BNDRY assumes a constant pressure of  $p_\infty$  over S for all time. Hence this represents a fallback option which will cause CALPROP to produce output identical to that from NASPROP-E. A second possibility occurs if  $NINT \leq NMAX$ , but NC is not an integral multiple of NINT. BIE will not get called on this step, and none of the boundary conditions on S are updated (though those on the nacelle will be). The third and final possibility is that  $NINT \leq NMAX$  and NC is an integral

multiple of NINT as well. This triggers a call to BIE as well as several other new routines unique to CALPROP which are used to correct the boundary conditions. Thus, if NINT = 3, BIE will be used to correct the conditions only every third time step, while for NINT = 1 the conditions are updated on every step. The other new routines that are called in addition to BIE and the functions they serve are described below.

The only other change made in BNDRY occurs when NC equals NMAX and is also a multiple of NINT. BNDRY then makes calls to NOISE (also described below) to compute the Sound Pressure Level, SPL, at those (RSIG, ZSIG) points inside the finite difference grid, and to the BIE package to get the SPL at points outside S.

#### New Routines Unique to CALPROP

These routines are called by BNDRY, directly or indirectly, when the step count NC is an integral multiple of NINT. They include OUTER, FRFIT, TRFORM, FREVAL, PR, and NOISE. We first give a brief description of each, followed by an explanation of how they interact. (The BIE package will be described separately.)

#### Subprogram

#### Description

OUTER	Evaluates $p$ and $\partial p / \partial n$ in physical space at the outer cylindrical surface needed for the acoustic field; once the acoustic solution is obtained, this routine also updates the pressure on the cylindrical interface accordingly.
FRFIT	Fits a Fourier series to $p$ and $\partial p / \partial n$ ; output is the set of Fourier coefficients.
TRFORM	Transforms Fourier coefficients of $p$ and $\partial p / \partial n$ between the physical and transformed space, the latter corresponding to no mean flow.

SubprogramDescription

FREVAL	Using the coefficients passed by BIE, this routine evaluates the Fourier series for p at the grid points on the cylindrical interface.
PR	A function subprogram which calculates static pressure at any grid point from the density, velocity components, and total energy stored in solution vector Q.
NOISE	Evaluates the Sound Pressure Level (SPL) for observer locations within the finite difference grid by interpolation.

All of these subprograms, except PR, contain the labelled COMMON/ACOUST/, which is their primary means of communication. No attempt has yet been made to vectorize them, as their run times are much smaller than the already existing NASPROP-E routines. A few are called with a single input parameter, IGO, whose value determines which of several logic paths is to be followed on that call. How these routines interact is best explained by recapitulating in sequence the steps described in Section 3 for communicating between NASPROP-E and BIE; at each step the routine responsible for its execution will be identified. In this way we are able to provide a convenient summary of the procedure, and the order of presentation will parallel the logic flow in the code.

A preliminary step is the initialization of various variables and arrays in COMMON/ACOUST/ and in BIE which can be calculated and stored once and for all. For this purpose NASPROP-E routine INITIA calls both routines OUTER and BIE with their input parameter IGO = 0. OUTER then calculates FSBETA, JMPKM and the wavenumber array WAVK; also arrays DELPHI and PHASE to be used subsequently in routines FRFIT and FREVAL.

The most important function served by this call to OUTER is the filling of arrays RTR and ZTR. These are the transformed coordinates  $\tilde{r}$ ,  $\tilde{z}$  of the outer grid points on S. They are obtained from NASPROP-E arrays Y and X,

corresponding to  $\bar{r}$  and  $\bar{z}$ , and Eq. (3-10a). RTR(I) and ZTR(I) are one-dimensional arrays whose index I = 1 at the lower left corner of Fig. 1 (J = 1, K = KMAX), and increases as one moves clockwise around the circumference, attaining its maximum value at the lower right (J = JMAX, K = 1), where I = JMAX + KMAX + 1. This is two more than the number of points actually on S, because at the corner points (J = JA, K = KMAX) and (J = JMAX, K = KMAX) the normal pressure gradient is double-valued. Hence the two points corresponding to I = JA and JA + 1 will have identical coordinates and pressures, but different values of  $\partial p / \partial n$ . The same is true of the two corner points corresponding to I = JMAX+1 and JMAX+2.

After exiting INITIA, and subsequently EIGEN (unchanged), CALPROP enters the main loop in Fig. 5, which is over the time step counter, NC. Each time NC is an integral multiple of NINT, the following sequence is triggered from BNDRY:

1. OUTER is called with input parameter IGO = 1. This signifies that arrays P and PN in labelled COMMON/ACOUST/ are to be filled with values for pressure and its normal derivative. Array P is filled by calling function PR for each outer grid point. PR simply solves Eq. (2-4) for p in terms of the stored values of density, velocity, and total energy. Array PN is filled by evaluating the appropriate form of Eq. (3-1) at each point, using second order accurate difference formulae for  $p_x$ ,  $p_y$  and  $p_z$ . The values for I = JA and JA + 1 will differ because of the switch from Eq. (3-1a) to (3-1b), as will the values for I = JMAX+1 and JMAX+2 because of the switch from Eq. (3-1b) to (3-1c).

2. FRFIT is called to do the Fourier decomposition. Equations (3-3) and (3-5) are approximated via the trapezoidal rule, using the discrete values of p and  $\partial p / \partial n$  stored in P and PN in Step 1. PHASE holds the necessary array of complex phase factors in Eqs. (3-3) and (3-5), and DELPHI the uneven increments in the abscissa,  $\Delta \phi$ . Both of these were computed in the initialization call to OUTER. The end result of FRFIT is the set of Fourier coefficients for pressure and its normal derivative, stored in arrays PC (MDUM,I) and PNC (MDUM,I) respectively. MDUM is an offset index for the mth harmonic, i.e.,  $m = MDUM-1$ ,  $1 \leq MDUM \leq MMAX+1$ ; again, I refers to a particular point on S.

3. TRFORM is called with the input parameter IGO = 1. This specifies that the routine is to compute the Fourier coefficients of the normal pressure gradient in the transformed variables by applying Eq. (3-16) to PC and PNC in physical space. The new transformed values are stored in array PNC, overriding those computed in Step 2.

4. BIE (discussed below) is called with input parameter IGO = 1. This signifies that the outer solution is to be obtained by inverting the appropriate integral equation, using the data in PNC as the inner boundary condition. BIE returns the solution for the pressure on S as a set of Fourier coefficients at the same grid points. The coefficients are stored in array PC, overriding those calculated in Step 2. Note again that BIE must essentially solve a separate problem for each of the harmonics,  $m=0,1..MMAX$ .

5. TRFORM is called again, this time with IGO = 2. This indicates that the Fourier coefficients returned by BIE, which are in the transformed variables, are to be converted back to physical space. TRFORM does so by applying Eq. (3-17) to array PC. The new values override those returned by Step 4 as they are computed.

6. FREVAL is called. The coefficients PC returned by Step 5 are those appropriate to Eq. (3-4) in physical space. FREVAL simply evaluates the Fourier series at all grid points on S. The resulting pressures are stored in array P, overriding those computed on Step 1.

7. OUTER is called again, this time with IGO = 2. Its job now is to use the newly estimated pressures from Step 6 to update the outer boundary conditions to be used on the next pass through NASPROP-E. First the new pressure values are relaxed using Eq. (3-18). The resulting values are used in Eq. (2-4) to compute new values for the total energy on  $S_A$  and  $S_B$ , assuming that the velocity components retain their free-stream values. The new energy values are stored in solution vector Q.

8. Control is returned to BNDRY, where the relaxed pressure values on the downstream surface  $S_C$  are used with the Method of Characteristics (Ref. 3) to calculate updated values for the density, velocity and energy. BNDRY also computes and prints out the r.m.s. change in pressure, as defined by Eq. (3-19).

9. If  $NC = NMAX$ , routine NOISE is called from BNDRY to compute the SPL at those observer locations, read in as coordinate pairs (RSIG, ZSIG), which lie within the finite difference grid. First, the quadrilateral cell in the computational  $(\xi, \eta)$  plane containing the observation point is identified. Then bilinear interpolation is used to get the pressure,  $PP(L)$ , at each of the corresponding azimuthal locations,  $PHI(L)$ ,  $L = 1 \dots LMAX$ . A Fourier decomposition is then performed on this data, again using a trapezoidal approximation like that in FRFIT, to yield the complex amplitude for the  $m$ th harmonic, stored as CP. Finally, the SPL is computed from

$$SPL = 20 \log_{10} |CPI|.$$

Since the pressures, and hence CP, have all been normalized by  $p_{\infty}$ , the above SPL is a relative scale referenced to  $p_{\infty}$ . To put it on an absolute basis once  $p_{\infty}$  and a reference pressure,  $p_{ref}$ , have been specified, one has merely to add the constant value,  $20 \log_{10} (p_{\infty} / p_{ref})$ . NOISE concludes by writing the coordinates of the observation point and the SPL predicted there for each harmonic. For observer positions outside the finite difference grid, the acoustic signal is computed with a call from BNDRY to BIE with input parameter IGO = 2.

#### Modified Mesh for the BIE

The BIE method involves integrations of kernels (e.g.,  $\exp(-ikR)/R$ ) which are of oscillatory nature. The oscillations increase with frequency. An estimate of the length for an element to perform satisfactorily accurate integrations can be determined. It is assumed that the kernel  $\exp(-ikR)/R$  can be integrated accurately, along with the shape functions, in an element of length equal to one-half the wavelength using five Gauss points per element. Thus, an element length of  $\pi/k$  is adequate. This is considered to be a conservative estimate of the element length.

The high frequencies ( $\tilde{k}R_S \gtrsim 100$ ) involved require much smaller element size than some of the elements in the NASPROP-E mesh. Since the BIE

code requires quadratic elements and the NASPROP-E mesh did not conform to such a mesh, it was decided to generate a new mesh based on the NASPROP-E mesh.

The NASPROP-E mesh is optimized for variations in boundary data, the nodes being crowded in regions of high gradients. Hence, it was decided to modify this optimal mesh rather than to generate a new mesh without consideration of boundary data.

It was also observed that the NASPROP-E mesh contains two distinct groups of two-noded elements, the "wide" and "narrow" elements. The elements longer than  $SMALEL=0.5$  ( $SMALEL$  may be changed as noted below) are considered to be wide elements and the rest as narrow elements. The NASPROP-E mesh also incorporates "dual nodes" at the corners of the cylinder. The BIE requires adjacent elements not to differ very much in length. Considering all these factors the following mesh generation scheme was adopted (see Fig. 6).

One of the dual nodes was dropped at each corner. One node was introduced in the narrow elements and an odd number of nodes ( $NPTS$ ) was introduced in the wide elements.  $NPTS$  is required to be an odd number so that an integral number of quadratic elements is generated in any wide element. One node was introduced in the narrow elements to make them quadratic elements. In this way, all the elements involved have their mid-nodes in the middle of the element. The narrow elements could not be combined (without addition of more nodes) into quadratic elements since an element might have been generated at the point of transition from the narrow to the wide elements, in which case the mid-node might have been very much off-center. This would cause singularity problems in the shape functions.

Extra elements of the same size as the last narrow element were introduced in the nacelle to close the grid, and  $\partial\phi/\partial n$  was prescribed to be zero on these elements. The given boundary data were approximated by a piecewise spline fit and the boundary data for the newly introduced nodes were determined.

#### Description of Routines in BIE

The block labelled BIE in Fig. 5 actually represents a package of several subprograms used to solve the outer acoustic field. A schematic of how

MODIFIED

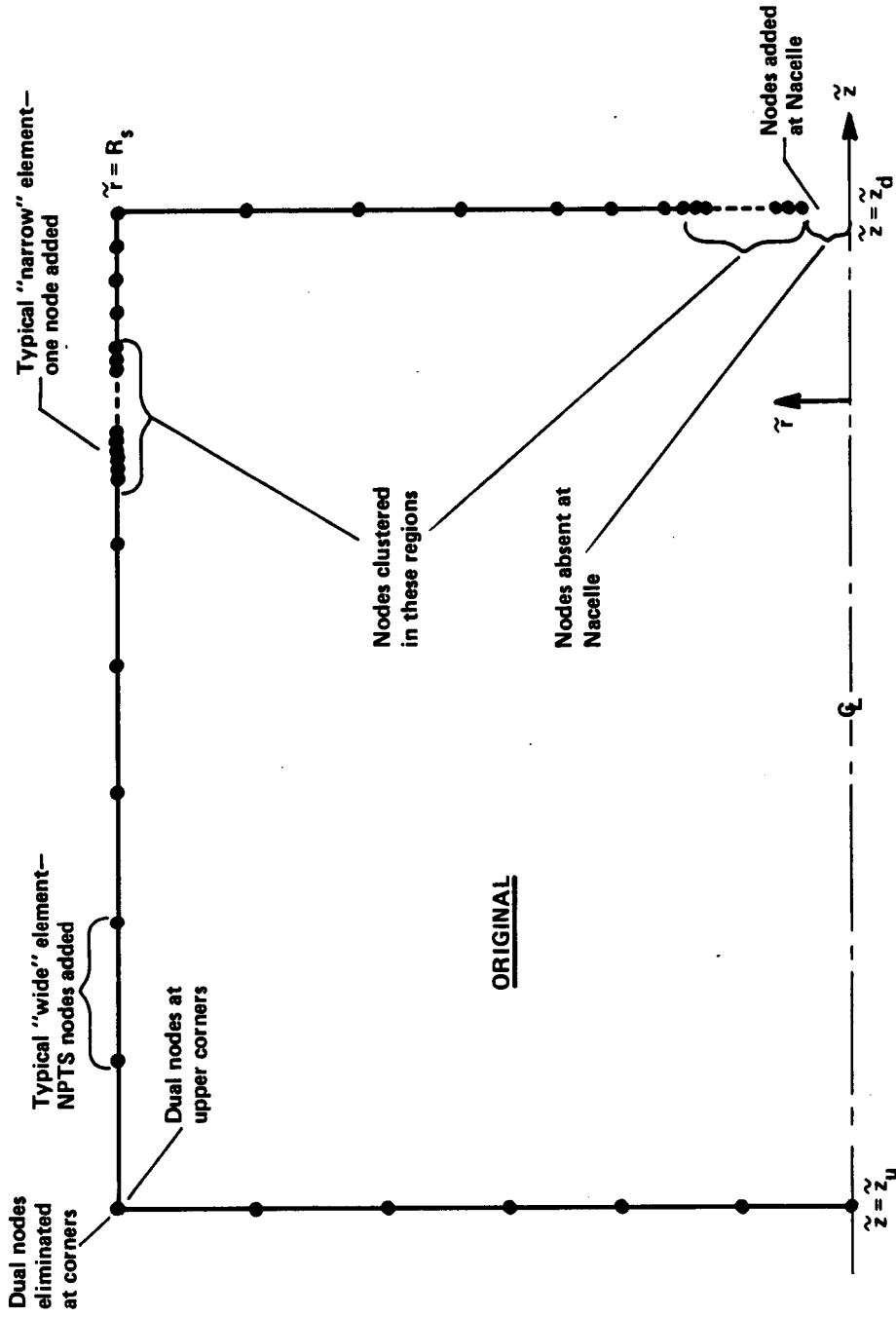


Figure 6. ORIGINAL AND MODIFIED NODE PLACEMENTS

they are interrelated is given in Fig. 7, and below is a brief description of the function served by each.

<u>Subprogram</u>	<u>Description</u>
BIE	Driver program for the rest of the package. IGO = 0 represents an initialization call; for IGO = 1 a new outer solution is obtained; for IGO = 2 the SPL at points outside the interface is computed based on the last solution.
SR1	Called only by BIE. Puts exterior coordinates (initially in arrays RTR & ZTR) into array XI.
SR2	Called only by BIE. This is the new mesh generation routine. Generates new nodes between existent nodes. Drops dual nodes at corners. Establishes node correspondence via arrays CORR1 and CORR2 between the given mesh and the new generated mesh. Introduces extra nodes in nacelle.
SR5	Called only by BIE. Calls SPLFIT and function FS. Interpolates the given boundary values of the given mesh to determine the same for all nodes of the new mesh. Also establishes the local-global node correspondence for the new mesh.
HEAX	Called only by BIE. Calls GAUSS, SHFUN, COEF, EXTR, SOLVER and BIVL. Solves for the unknown surface and field pressures using the BIE method.
SR6	Called only by BIE. Calculates the Sound Pressure Level.
FILLPC	Called only by BIE. Fills array PC, i.e., finds the Fourier pressure coefficients on the surface at the nodes of the given mesh.

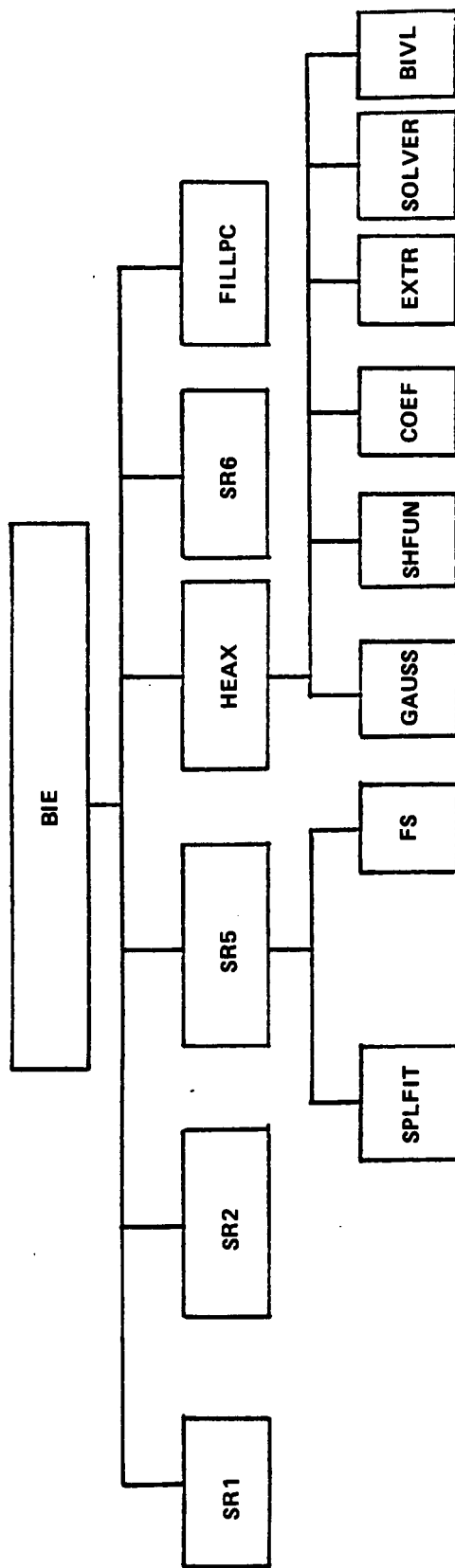


Figure 7 HIERARCHY CHART FOR THE BIE PACKAGE

<u>Subprogram</u>	<u>Description</u>
GAUSS	Calculates abscissas and weight factors for numerical (Gaussian) quadrature.
SHFUN	Calculates and stores values of shape functions and their derivatives for quadrature.
COEF	Calculates and stores the matrix of coefficients and the known (i.e., $\partial\tilde{p}/\partial\tilde{n}$ ) vector.
EXTR	Modifies the matrix of coefficients and the known vector for exterior problems.
SOLVER	Solves the system of linear algebraic equations.
BIVL	Prints nodal values of $\tilde{p}$ and $\partial\tilde{p}/\partial\tilde{n}$ and prints the values of pressure at exterior points.
SPLFIT	Interpolates $\partial\tilde{p}/\partial\tilde{n}$ to get cubic spline coefficients.
FS	Uses spline coefficients from SPLFIT to determine $\partial\tilde{p}/\partial\tilde{n}$ at additional nodes.

#### Description of Important Parameters in BIE

The following are major parameters governing the operation of the BIE solution:

<u>Variable</u>	<u>Description</u>
NG	Number of Gauss points per element for integrations along the generator when both source and field points are on the surface. Maximum value is 10.

<u>Variable</u>	<u>Description</u>
NGG	Number of Gauss points per element for integrations in the direction of the angle of revolution. Maximum value is 10.
NPTS	Number of nodes introduced in every wide element in NASPROP-E grid. Must be an odd number.
NSS	Number of subdivisions (elements) in $\pi$ radians in the direction of revolution.
SMALEL	A length such that elements of NASPROP-E grid longer than this length are classified as "wide" elements. A value of 0.5 is suggested.

The first four parameters are related - all affect the numerical accuracy. We recommend setting NG and NGG to a value between 5 and 10. When this is done we have found that a conservative element (subdivision) length is given by  $\pi/k$  where k is the wavenumber. This criterion can be used to select NPTS and NSS such that high numerical accuracy is achieved. Using the  $\pi/k$  criterion we determine NSS by:

$$NSS = \frac{\text{one-half of circumference of cylinder}}{\pi/k} + 1,$$

$$NSS = 5k + 1 ,$$

since  $R_S=5$  is the radius of the cylinder. The 1 in the above equation insures that there is a single subdivision in  $\pi$  radians in the direction of revolution when  $k=0$  (i.e. the  $m=0$  term of the Fourier series). We use the same  $\pi/k$  criterion to determine the maximum element length along the generator. We do this by selecting the wide element with the maximum length ( $\approx 1$ ), divide this length by  $\pi/k$  and pick NPTS accordingly (noting that NPTS must be an odd number). The relationship between k, NPTS and the total number of nodes on the generator is given below (for SMALEL = 0.5).

$k\pi$	NPTS	TOTAL NUMBER OF NODES
$\pi$	1	139
$2\pi$	3	161
$3\pi$	5	183
$4\pi$	7	205
$5\pi$	9	227
$6\pi$	11	249
$7\pi$	13	271

Section 6  
RESULTS

We have not been able to get the new CALPROP code to run a case through to completion, and so have little in the way of numerical results to report. Basically, the code takes too long to execute. In the discussion below, we will first describe the sample case we have been working on, followed by a description of the difficulties we encountered.

Figure 8 displays the input data as printed by the code for the case we worked with, corresponding to an eight-bladed SR-3 propeller at a nominal flight Mach number of 0.8. The angle of attack is  $0^\circ$  (neither NASPROP-E nor the BIE package can handle the asymmetric inflow case), and the advance ratio is 3.06. The finite difference grid used was that generated for us by H. Huynh (cf. Section 2) based on the SR-3 blade geometry and the new cylindrical outer boundary. Referring to Fig. 1, the radius of the outer boundary was set at  $R_S = 5$  propeller diameters. The upstream and downstream faces of the cylinder were put at  $z_u = -5$  and  $z_d = 1.05$ . In the coordinate system used by the outer solution, these transform to  $\tilde{z}_u = -8.33$  and  $\tilde{z}_d = 1.75$ . The grid has  $JMAX = 45$  points in the  $\xi$  direction,  $KMAX = 21$  in the  $\eta$  direction, and  $LMAX = 11$  in the  $\zeta$  direction (not shown). The line of constant  $\xi$  intersecting the upper left-hand corner of the cylindrical interface is at  $J = JA = 7$ . The grid point coordinates of this mesh can be accessed through permanent dataset name OURMESH with ID = FSSPAN. Because this was to be a demonstration run, the maximum number of iterations (time steps) asked for was only  $NMAX = 5$ . A Courant number of 20 was specified for calculating the step size used by the ADI difference scheme.

The new input parameters unique to CALPROP are listed near the end in Fig. 8.  $NINT = 1$  specifies that the BIE package is to be called on each time step to update the outer boundary conditions applied to the inner flow.  $MMAX = 2$  specifies that the  $m = 0, 1$  and  $2$  Fourier components are to be included in the acoustic calculation. These correspond to the steady-state component, the fundamental blade passage frequency, and its first harmonic, respectively, cf. Eq. (3-7). This is considered minimal; the program is dimensioned to

MACH NO.= 0.80  
ANGLE OF ATTACK= 0.00 DEGREES  
RATIO OF SPECIFIC HEATS=1.4  
PINF=0.1000E+01  
RHOINF=0.1000E+01  
ADVANCE RATIO =-0.30600000E+01  
BETA 3/4= -58.70 DEGREES  
BLADE DIAMETER= 1.00 FEET  
OMEGA= -0.31 REVOLUTIONS PER SECOND  
NO. BLADES= 8  
PERIOD = 45.00000RADIAN  
JMAX=45  
KMAX=21  
LMAX=11  
ITERATIONS= 5  
METHOD=2 (1=EXPLICIT, 2=IMPLICIT)  
COURANT NO.=20.00  
4TH ORDER SMOOTH CONST=0.1000  
2ND ORDER DISSIP CONST=0.2000  
DIFFERENCING METHOD=4 (2=SECOND ORDER,4=FOURTH ORDER)  
IREAD=0  
IWRT=1  
IPTCH=1  
JLE=20  
JTE=35  
KTIP=12  
IBC= 0  
INETOT= 0  
NCHNGE= 9000  
IGRID= 1  
NINT = 1  
MMAX = 2  
NSIG = 1  
JA = 7  
EPS = 1.000E-02  
RLXBC = 1.000

Figure 8 INPUT DATA FOR DEMONSTRATION CASE

allow MMAX to be as large as 5. Values of the other input parameters are not critical to the following discussion.

After first mating the NASPROP-E and BIE codes together with the new routines required for the matching (Section 5), it was found that the combined CALPROP code would not execute. What ensued was a period of several months during which a series of trial-and-error runs were made to "get the bugs out." These included an initial incongruity between NASPROP-E and the new fully cylindrical grid, subtle logic errors which passed muster at compile time but raised havoc during execution, and incompatibilities between NASPROP-E and BIE which became evident only when passing information between the two. Without going into detail, suffice it to say that this initial debugging period took many times longer than anticipated.

In our defense, we should point out that NASPROP-E and BIE were developed independently for somewhat different purposes, and on different systems at that. Our efforts were also hampered by the geographical separation between ourselves and Prof. Seybert, the time needed to familiarize ourselves with the idiosyncrasies of the NASA/Lewis CRAY operating system, and the limitations imposed on us by having only remote access to the system. The limited number of telephone access ports relative to the apparently large community of users pretty much restricted our useful window of access to the CRAY to a few very early-morning hours.

Our preliminary development efforts have now brought us to the point where the code runs, but a more serious obstacle has been encountered. This was discovered when a run bombed for having exceeded our self-imposed job time limit of 100 secs., without completing the first time step. As a point of reference, the original NASPROP-E code completed 10 time steps in approximately 12 sec. using the same finite difference grid. We activated the TRACEBACK option on subsequent runs, and added internal diagnostic messages to let us know which of the new routines unique to CALPROP had been successfully exited. This pinpointed the problem to routine COEF, part of the BIE package supplied by Prof. Seybert, which was entered but never exited. (This was the first time the code had gotten far enough along to call COEF.) As a further check we also made a run in which the entire BIE subroutine package was removed and replaced with

a "dummy" BIE routine that simply filled the PC array with the complex constant (1.0, 1.0). Though the results were meaningless, the modified code made it through two complete time steps in a few seconds. This demonstrated that the other new routines in CALPROP (dashed outline in Fig.5) ran in a reasonable amount of time.

Our initial suspicion was that perhaps a DO LOOP parameter in COEF had been left undefined, and the code was looping ad infinitum. A careful inspection of the COEF structure turned up the following set of five nested DO LOOPS:

```
      DO 500 K = 1,M
      DO 100 IG = 1, NG
      .
      .
      .
      DO 90 IR = 1,N
      .
      .
      .
      DO 515 IJ = 1,NS
      DO 51 IIG = 1 1,NGG
      .
      .
      .
51 CONTINUE
515 CONTINUE
      .
      .
      .
90 CONTINUE
100 CONTINUE
      .
      .
      .
500 CONTINUE
```

A system timing routine was added to COEF on an ad hoc basis, which confirmed that the program was in this section of code when it ran out of time. The symbolic dump triggered by the TRACEBACK disclosed that  $M = 89$ ,  $NG = 10$ ,  $N = 179$ ,  $NS = 80$  and  $NGG = 10$ . This means that the block of statements within the innermost loop would have to be executed approximately  $1.3 \times 10^8$  times. The block contains on the order of  $10^2$  floating-point operations, which is probably on the low side. Hence a total of  $1.3 \times 10^{10}$  operations are needed; assuming a sustained rate for the CRAY of  $2 \times 10^7$  floating-point operations per second, this section of code alone would require in excess of 10 min. CPU time.

The above estimate is just for one Fourier component at one time step. For the present demonstration case which includes only three Fourier components, and assuming that on the order of 100 time steps would be needed to converge (typical of the original NASPROP-E code, cf. Ref. 3, p. 100), something in excess of 53 hrs. of CRAY time would be required to get one solution. Admittedly this is only a ballpark figure, but it is clearly unacceptable even for a research oriented code.

COEF is not a peripheral routine which can be temporarily bypassed. It is at the heart of the BIE package, in that it calculates the coefficient matrix in the set of linear equations to which the original integral equation is transformed by the discretization. The elements of the coefficient matrix involve quadratures in two dimensions over the cylindrical interface. It is these quadratures, for each of the  $M$  elements on the generator of the cylinder, which are being done in this nested loop construct. Parameters such as  $NGG$ ,  $NS$ , etc., refer to the number of Gauss quadrature points and subdivisions to be used in the integrations (cf. Section 5).

We consulted Prof. Seybert regarding our problem, who felt in retrospect that perhaps he had been overly conservative in choosing the number of discretization elements and Gaussian quadrature points. As a result, the BIE package was restructured so that a different number of interface elements and azimuthal subdivisions was used for each frequency (the lower the wavenumber, the coarser the grid), and  $NG$  and  $NGG$  were both reduced from 10 to 5.

Another attempt was made with these changes to CALPROP, and this time the first call to COEF was successfully completed for the  $m = 0$  (i.e., steady-state) Fourier component in only 15 sec. However, for the  $m = 1$  component (the fundamental blade passage frequency), the code again bogged down in COEF and ran out of time, taking 175 sec. just to complete the  $K = 6$  pass through the outermost loop, out of the 129 passes required. On this call,  $M = 129$ ,  $NG = 5$ ,  $N = 259$ ,  $NS = 10$ , and  $NGG = 5$ , for a total of approximately  $4 \times 10^7$  passes through the innermost loop. This represents only a marginal improvement from the previous run, and does not augur well for what would be required if it ever got to the  $m = 2$  harmonic.

Thus in its present form the CALPROP code can be made to run in some sense, but it is economically unfeasible to use. This is not because of any known errors per se, nor is the problem amenable to a "quick fix" resolution. The way the code is structured, it simply generates such a volume of arithmetic for the outer solution that it overtaxes the capabilities of even a CRAY. Unfortunately, at the point this was discovered there was neither the time nor resources remaining to do any major restructuring of the BIE package. More will be said about this in the next section.

## Section 7

### CONCLUSIONS AND RECOMMENDATIONS

Since we were not able to get any converged solutions with CALPROP, no meaningful conclusions can be drawn regarding the aerodynamics and acoustics of advanced propfans per se. Nevertheless, we still feel strongly that such a hybrid numerical scheme is a viable approach for such predictions, and would like to offer some comments that may prove useful to future investigators.

This is the type of problem that would ordinarily form the basis for a long-term program of developmental research. Instead, because of time and manpower limitations, we were forced to turn to "off-the-shelf" software wherever possible. In retrospect we may have been overly optimistic in thinking we could easily marry two such disparate codes as NASPROP-E and BIE. Each had originally been developed for independent purposes, and on different systems. NASPROP-E was attractive because it was under no proprietary restraints, and the mechanics of how to fold in the complex SR-3 blade geometry had already been done for us. Similarly, BIE was chosen because it was readily available, and had already been used with a finite cylindrical boundary.

But neither code had been designed to communicate with another. Hence there were many inconsistencies between the two, some documented and some not, that had to be ironed out on an ad hoc basis. This and the logistical problems introduced by the long-distance collaboration with Prof. Seybert, and having only remote access to the CRAY system, diverted too much effort away from the real technical issues. Ideally, a program of this complexity should command sufficient resources that the inner and outer flow solution packages would be developed in concert, on the same system, with the task of communication between the two always kept uppermost in mind.

Having said that, there remain two obstacles to further development of the CALPROP code, viz., its very large run times, and the potential ill-conditioning of the outer solution near the interior eigenfrequencies (Section 4). The root cause of the run time problem is routine COEF, which calculates the coefficient matrix in Eq. (4-27) anew at each time step. Yet there is no reason to do so, since the matrix depends only on the acoustic

frequency and the node placement, which remain fixed. It is only the right-hand side vector in Eq. (4-27), which contains the boundary conditions, that must be updated on each iteration. Hence it is recommended that BIE be restructured so that the matrix is calculated and stored once and for all at the beginning of a run, preferably on the initialization call from INITIA with IGO = 0. Since a separate matrix must be stored for each Fourier component, this will greatly increase storage requirements. But with the memory available on the CRAY it should prove feasible, and the savings in run time would be tremendous.

Even with only a single calculation of the coefficient matrices, the timing statistics quoted in Section 6 suggest that the run time might still be large. Further reductions could be gained by reducing the number of nodes used on the interface, and hence the size of the matrices, in the outer solution. The BIE package presently uses the grid intersection nodes from NASPROP-E as a starting point, and then inserts extra nodes between them as needed, cf. Section 5 and Fig. 6. This is done to avoid abrupt transitions from closely to widely spaced nodes, which causes problems in the BIE method. But even the modified node structure that results is hardly optimal from the BIE viewpoint. It is suggested that a better approach is to base the node placement for the outer flow primarily on the needs of that solution, more or less independently of the grid points used in the inner flow. Cubic splines could be easily used to transfer data from one set of points to the other as needed. Such a scheme should allow fewer nodes for the BIE solution, and reduced run times.

These last two points, i.e., when should the BIE matrices be calculated and for what node distribution, are good examples of the problems that arose because BIE was originally developed with other applications in mind. It had previously been applied only to comparatively coarse grids, where the boundary conditions had a very simple variation that was prescribed a priori; hence no iterations were necessary. Run times were minimal, so that considerations of computational efficiency such as those above never arose.

Assuming the time needed for the outer solution can be reduced sufficiently, that still leaves the question of nonuniqueness. That is, the matrix equation for the exterior Neumann (Dirichlet) problem is known to be strongly ill-conditioned near the eigenfrequencies of the complementary interior

Dirichlet (Neumann) problem. As discussed in Section 4 for the frequency range of interest here,  $\tilde{k}R_S \gtrsim 100$ , the eigenfrequencies are much too closely spaced to get solutions by simply "tweaking"  $\tilde{k}$  until it lies between adjacent eigenfrequencies. For the present program the CHIEF method (Refs. 18, 21) was chosen as the most promising scheme to overcome this difficulty. Test cases have been run for simple point sources within the same cylindrical interface used here, but to date accurate solutions have only been obtained up to  $\tilde{k}R_S \approx 20$ . This is well below the range needed for even the fundamental blade passage frequency, which for the case cited in Section 6 is  $\tilde{k}_1R_S = 109.5$ . For this reason the additional routines required to implement CHIEF are not presently included in CALPROP.

Professor Seybert's statements at the end of Section 4 notwithstanding, the author believes that the method used by Meyer, et al. in Ref. 22 is a preferable means of removing the ill-conditioning. They solve a modified integral equation, formed as a linear combination of the original equation and its derivative normal to the interface. The new equation has been shown to possess a unique solution at all wavenumbers. Numerical results presented in Ref. 22 confirm this, even at conditions coincident with the interior eigenfrequencies. This method was successfully implemented by Baumeister and Horowitz (Ref. 10) in a similar hybrid scheme applied to turbofan inlet acoustics. A finite element solution was applied to the inner nonlinear flow. The boundary integral method of Ref. 22 was used for the linearized acoustic field. Assuming (conservatively) that the radius of their interface was at the outer surface of the nacelle, for their blade passage frequency  $\tilde{k}_1R_S \approx 35$ . The computed results were obtained with only 59 boundary segments and show no evidence of ill-conditioning. Reasonable agreement with experimental data was also demonstrated.

The nonuniqueness of the solution to Eq. (4-12) near the eigenfrequencies is not a manifestation of any physical phenomenon. It is a purely mathematical artifact introduced by the transformation of the governing equation from differential to integral form. The fact that the problem gets progressively worse with increasing frequency should perhaps suggest to us that we may be attacking it from the wrong direction. That is, for the regime of

interest here we may not need the full-blown BIE artillery, if only we are clever enough to somehow take advantage of the short wavelengths.

Such a high frequency approximation has been used successfully in studying radiation from solid bodies, e.g., Ref. 23 and 24. In the high frequency limit the waves behave asymptotically like plane waves. This together with the condition of no flow through the wall leads to a simple algebraic relation between the acoustic pressure and the velocity normal to the surface, which in effect can serve as a boundary condition replacing the integral equation.

Such an approximation was briefly considered here, until it was realized that this simple relation would not apply in our case because the surface is not solid. For a solid radiator in this limit, the normal to the surface is also normal to the acoustic wave fronts; but in the present problem there is no reason for this to be so, as waves can pass through the interface at any angle. This added degree of freedom destroys the simple algebraic relation. However, it may be that with enough thought a more general relation could be worked out. The possibility of such an approach at high frequencies is very attractive, as it not only removes any ill-conditioning, but obviates altogether the need to invert an integral equation.

In summary, the lack of success in the present investigation should not be taken as evidence that the basic approach is unworkable. A hybrid scheme matching an inner nonlinear flow to an outer linearized field still appears ideally suited to predicting the aerodynamic and acoustic fields of advanced turboprops. It is hoped that the comments offered here will help to further progress toward that goal.

## REFERENCES

1. Dittmar, J.H. and Lasagna, P.L., A Preliminary Comparison Between the SR-3 Propeller Noise in Flight and in a Wind Tunnel, NASA TM 82805, 1982.
2. Dittmar, J.H., A Comparison Between an Existing Propeller Noise Theory and Wind Tunnel Data, NASA TM 81519, 1980.
3. Chaussee, D.S. and Kutler, P., User's Manual for Three-Dimensional Analysis of Propeller Flow Fields, NASA CR 167959, 1983.
4. Bober, L.J., Chaussee, D.S. and Kutler, P., Prediction of High Speed Propeller Flow Fields Using a Three-Dimensional Euler Analysis, NASA TM 83065, (also as AIAA Paper 83-0188), 1983.
5. Seybert, A.F., Soenarko, B., Rizzo, F.J. and Shippy, D.J., Application of the BIE Method to Sound Radiation Problems Using an Isoparametric Element", ASME Transactions, Journal of Vibration, Acoustics, Stress and Reliability in Design, Vol. 106, July, 1984, pp. 414-420.
6. Beam, Richard M. and Warming, R.F., "An Implicit Finite-Difference Algorithm for Hyperbolic Systems in Conservation-Law Form," J. of Comp. Physics, Vol. 22, 1976, pp. 87-109.
7. Pulliam, T.H. and Steger, J.L., "On Implicit Finite-Difference Simulations of Three-Dimensional Flow," AIAA J. Vol. 18, No. 2, Feb. 1980, pp. 159-167.
8. Pulliam, T.H., and Chaussee, D.S., "A Diagonal Form of an Implicit Approximate-Factorization Algorithm," J. of Computational Physics, Vol. 39, No. 2, 1981, pp. 347-363.
9. Warming, R.F., Beam, R.M., and Hyett, B.J., "Diagonalization and Simultaneous Symmetrization of the Gas Dynamic Matrices," Math. Comp., Vol. 29, No. 132, Oct. 1975, pp. 1037-1045.
10. Baumeister, K.J. and Horowitz, S.J., "Finite Element-Integral Acoustic Simulation of JT15D Turbofan Engine", ASME Transactions, J. of Vibration, Acoustics, Stress and Reliability in Design, Vol. 106, July 1984, pp. 405-413.
11. Tester, B.J., "The Propagation and Attenuation of Sound in Lined Ducts Containing Uniform or Plug Flow", J. of Sound and Vibration, Vol. 28, No. 2, May 1973, pp. 151-203.
12. Baker, B.B. and Copson, E.T., The Mathematical Theory of Huygen's Principle, Part I, McGraw-Hill, 1939.
13. Sears, W.R., Vidal, R.J., Erickson, J.C., Jr., and Ritter, A., "Interference-Free Wind Tunnel Flows by Adaptive-Wall Technology," Journal of Aircraft, Vol. 14, No. 11, Nov. 1977, pp. 1042-1050.
14. Rizzo, F.J., and Shippy, D.J., "The Boundary Integral Equation Method with Application to Certain Stress Concentration Problems in Elasticity", J. Austral. Math. Soc. (Series B), Vol. 22, 1981, pp. 381-393.

15. Shaw, R.P., "Boundary Integral Equation Method Applied to Wave Problems", Developments in Boundary Element Methods Vol. 1, P.K. Banerjee and R. Butterfield, (Eds.), Applied Science Publishers Ltd., London, 1979, Chapter 6.
16. Morse, P.M., and Feshbach, H., Methods of Theoretical Physics, Part 1, McGraw-Hill, New York, 1953, Chapter 7.
17. Skudrzyk, E., The Foundations of Acoustics, Springer-Verlag, New York, 1971, Chapters 23 and 27.
18. Schenck, H.A., "Improved Integral Formulation for Acoustic Radiation Problems", J. Acoust. Soc. Am., Vol. 44, No. 1, 1968, pp. 41-58.
19. Piaszczyk, Christopher M., "Acoustic Radiation from Vibrating Surfaces at Characteristic Frequencies", J. Acoust. Soc., Am., Vol. 75, No. 2, 1984, pp. 363-375.
20. Soenarko, B., "An Advanced Boundary Element Formulation for Acoustic Radiation and Scattering in Three Dimensions", Ph.D. Dissertation, Department of Mechanical Engineering, University of Kentucky, 1983.
21. Koopman, G.H. and Benner, H., "Method for Computing the Sound Power of Machines Based on the Helmholtz Integral", J. Acoust. Soc. Am., Vol. 71, 1982, pp. 78-79.
22. Meyer, W.L., Bell, W.A., Stallybrass, M.P. and Zinn, B.T., "Prediction of the Sound Field Radiated from Axisymmetric Surfaces", J. Acoustical Society of America, Vol. 65, No. 3, March 1979, pp. 631-638.
23. Lax, M. and Feshbach, H., "On the Radiation Problem at High Frequencies", J. Acoustical Society of America, Vol. 19, No. 4, July 1947, pp. 682-690.
24. Huang, H., "Helmholtz Integral Equations for Fluid-Structure Interaction", in Advances in Fluid-Structure Interaction, eds. Everstine, G.C. and Au-Yang, M.K., ASME AMD - Vol. 64, 1984, pp. 19-38.

## NOMENCLATURE

a	speed of sound
$A_m, B_m, C_m$	dimensionless Fourier coefficients of pressure distribution over $S_A, S_B, S_C$ ; defined by Eq. (3-5)
$\tilde{A}_m, \tilde{B}_m, \tilde{C}_m$	dimensionless Fourier coefficients of pressure distribution in transformed variables; related to the above by Eq. (3-17)
$A_m^n, B_m^n, C_m^n$	dimensionless Fourier coefficients of the normal pressure gradient over $S_A, S_B, S_C$ ; defined by Eq. (3-3)
$\tilde{A}_m^n, \tilde{B}_m^n, \tilde{C}_m^n$	dimensionless Fourier coefficients of the normal pressure gradient in transformed variables; related to the above by Eq. (3-16)
B	number of blades
D	propeller diameter
e	total energy per unit volume normalized by $p_\infty$ ; defined in Eq. (2-4)
E, F, G	flux vectors in the $\xi, \eta, \zeta$ directions, respectively; defined in Eq. (2-6)
G	Green's function defined in Eq. (3-12)
H	vector of undifferentiated source terms defined by Eq. (2-8)
J	Jacobian of the generalized coordinate transformation defined by Eq. (2-5)
J, K, L	integer grid indices in the $\xi, \eta, \zeta$ directions
JMAX, KMAX, LMAX	maximum values of the above

$k_m$	dimensionless wavenumber of mth harmonic, normalized by $D^{-1}$
$M$	free-stream Mach number
$m$	Fourier series (harmonic) index
$n$	local outward normal to the interface surface $S$ in Fig. 2
$p$	dimensionless static pressure normalized by $p_\infty$
$\tilde{p}$	dimensionless static pressure in transformed variables; related to $p$ by Eq. (3-10b)
$Q$	vector of dependent variables in finite difference solution, Eq. (2-3)
$R_S$	dimensionless radius of surface $S_B$ , normalized by $D$
$S_A, S_B, S_C$	upstream, sidewall, and downstream faces, respectively, of cylindrical interface $S$ , Fig. 2
$t$	dimensionless time normalized by $D\sqrt{\gamma}/a_\infty$
$u, v, w$	dimensionless velocity components in the $z, r, \phi$ directions normalized by $a_\infty/\sqrt{\gamma}$
$U, V, W$	dimensionless contravariant velocity components in the $\xi, \eta, \zeta$ directions normalized by $a_\infty/\sqrt{\gamma}$ ; defined by Eq. (2-7)
$z, r, \phi$	dimensionless cylindrical blade-fixed coordinates normalized by $D$
$\bar{z}, \bar{r}, \bar{\phi}$	dimensionless cylindrical coordinates translating with the propeller, but not rotating; related to the above by Eq. (3-6)
$\tilde{z}, \tilde{r}, \tilde{\phi}$	dimensionless cylindrical coordinates used in transformation to no mean flow; related to the above by Eq. (3-10a)

$\bar{z}_u, \bar{z}_d$	dimensionless axial coordinates of $S_A$ and $S_C$ , Fig. 2
$\alpha$	relaxation factor used in updating the boundary conditions on S, Eq. (3-18)
$\beta$	$\sqrt{1-M^2}$
$\gamma$	specific heat ratio
$\delta$	Dirac delta function
$\epsilon$	convergence criterion, Eq. (3-19)
$\xi, \eta, \zeta$	generalized boundary-conforming coordinates, Eq. (2-1)
$\rho$	dimensionless density normalized by $\rho_\infty$
$\Omega$	dimensionless angular velocity of the propeller, normalized by $a_\infty / (D\sqrt{\gamma})$ .

Superscripts

n	used to indicate Fourier coefficient of the normal pressure gradient, e.g. $A_m^n$
q	time index in Eq. (3-18)
T	indicates the transpose of a vector, e.g. Eq. (2-3)

Subscripts

m	pertaining to the mth harmonic of Blade-Passage Frequency
i	pertaining to the inner flow solution
o	pertaining to the outer flow solution
o	denotes a source point on S in Eq. (3-13)
$\infty$	evaluated at upstream infinity